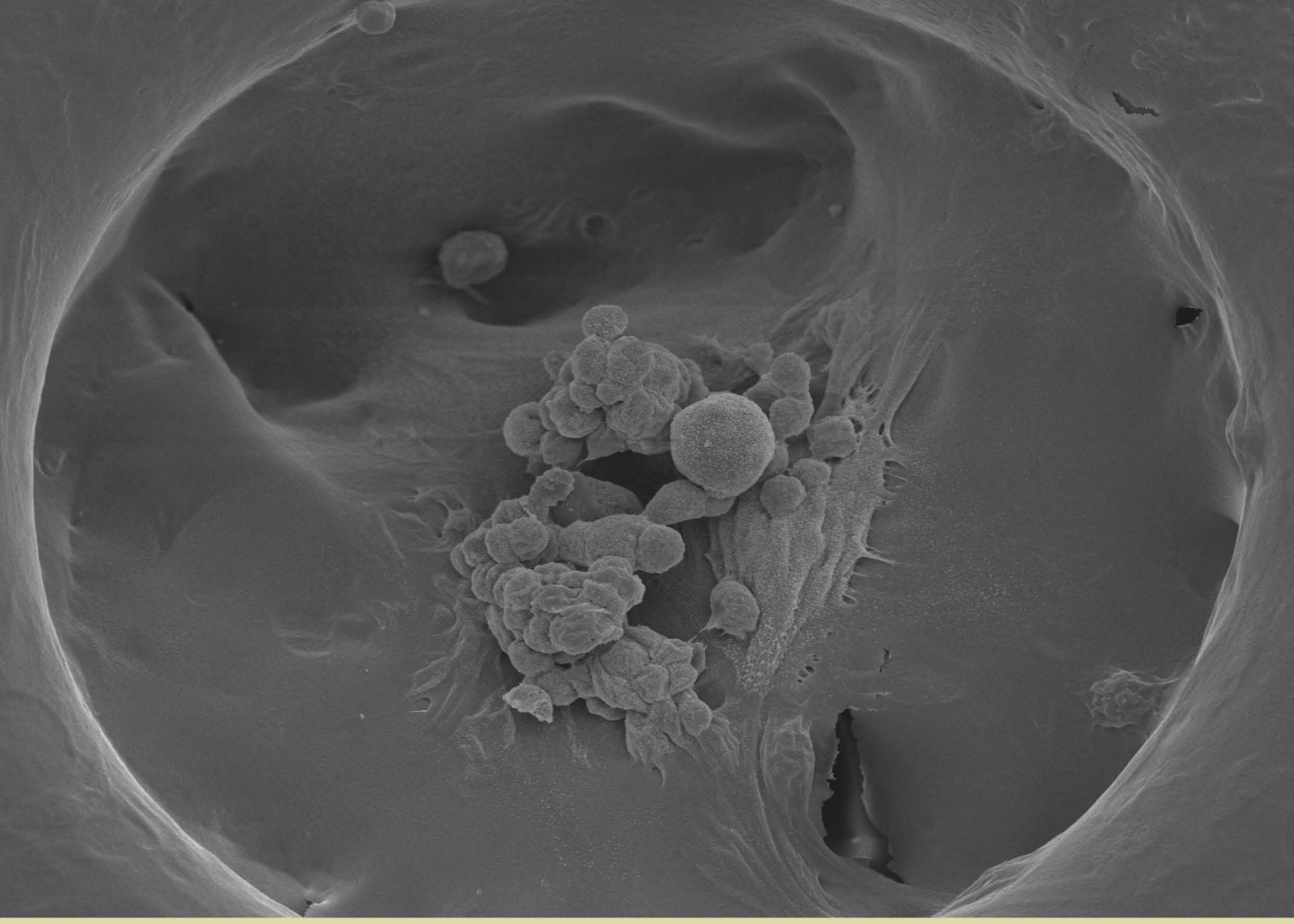

Sara Vilabril Ramos

Microengineered 3D *in vitro* Model of Human Pulmonary Alveoli: Curvature's Influence on Lung Epithelial Cells

Thesis submitted to the University of Coimbra in compliance with the requirements for the degree of Master in Biomedical Engineering

September 2017

· U C ·

Universidade de Coimbra

• U C •

FCTUC FACULDADE DE CIÊNCIAS
E TECNOLOGIA
UNIVERSIDADE DE COIMBRA

Sara Vilabril Ramos

Microengineered 3D *in vitro* Model of Human Pulmonary Alveoli: Curvature's Influence on Lung Epithelial Cells

Thesis submitted to the
University of Coimbra for the degree of
Master in Biomedical Engineering

Supervisors:
Prof. Dr. Roman Truckenmüller (MERLN, Maastricht University)
Prof. Dr. Jorge Coelho (University of Coimbra)

Coimbra, 2017

This work was developed in collaboration with:

MERLN

Institute for Technology Inspired Regenerative Medicine

Maastricht University

· U  C ·

Universidade de Coimbra

Acknowledgments

To Dr. Roman and Dr. Stefan my sincere gratitude for accepting me in your research group and for giving me this life changing experience. Thank you for always having time to help me, to clarify any doubt I had and for all the times you just asked how I was doing. You are a true inspiration as professionals and as human beings .

To my daily supervisor, Danielle Baptista, thank you for letting me make part of your amazing and challenging project. Thank you so much for everything you taught me and for making me believe in my work, in my personal value, and for encouraging to be more and more independent everyday.

To my supervisor from University of Coimbra, Dr. Jorge Coelho, I'll never be able to thank you enough for helping me pursuing my dream of developing my master's thesis at MERLN and for always being available to help me and advise me with anything I needed.

My gratitute to Prof. Clemens van Blitterswijk for providing me the opportunity to work and develop my master's thesis at the Department of Complex Tissue Regeneration of MERLN Institute for Technology-Inspired Regenerative Medicine.

To Dr. Liliana Moreira Teixeira and Pinak Samal, my true appreciation for helping me and teaching me when I needed. To Ana Luísa, Silvia, David, Víctor, Estela, Erik and all MERLN family, I will never forget the amazing months we shared and everything I learnt from you.

To Lluís, words are not enough to thank you for all you did for me in Maastricht. Thank you for sharing so many funny moments, laughs and for helping me when I needed the most. Our bond is eternal. To my sweet Onder de Kerk girls, Dudu and Rosa, thank you for all the amazing moments in the kitchen! You were my family away from home.

To my special girls, my family in Coimbra, thank you for these incredible 5 years

and for all good memories we share. This was just the beginning! To my amazing friends from Coimbra, thank you for making this city so special.

To my boyfriend and best friend, João, thank you from the bottom of my heart for always being there for me, no matter what. My honest gratitude for always putting a smile on my face, for motivating me, for listening to my random thoughts, for never allowing me to give up and for all the effort you made to make distance look like nothing. I wouldn't be able to finish this thesis without your strength and love.

Aos meus pais, Carlos e Victória, e à minha irmã, Filipa, o meu mais sincero agradecimento por serem os meus pilares, a minha maior inspiração e por acreditarem, constantemente, no meu valor. Obrigada por estarem sempre presentes, nos bons e nos maus momentos, e por me mostrarem que é preciso lutar, diariamente, para conseguirmos alcançar os nossos objectivos. Esta tese é dedicada a vocês.

Resumo

A engenharia de tecidos visa criar modelos *in vitro* de tecidos e estruturas biológicas funcionais recorrendo a diferentes tecnologias, conforme o objectivo final. Uma estratégia importante para adquirir um bom conhecimento do funcionamento dos órgãos humanos e da sua interações enquanto sistema biológico passa por devenvolver modelos *in vitro* que representem, da melhor forma possível, a sua anatomia e fisiologia.

No caso particular desta dissertação, de forma a criar uma representação realista do alvéolo humano é necessário desenvolver um modelo *in vitro* 3D obtido por microengenharia que contenha características dimensionais semelhantes às do órgão a ser modelado (profundidade aproximadamente 100μm e diâmetro 200μm [1][2][3]). Nos últimos anos, um grande ênfase tem sido dado aos modelos pulmonares *in vitro*, os quais têm sido melhorados pela passagem de conformação 2D para 3D, como o caso de organóides pulmonares [4], mas nenhum modelo na literatura relata o uso de curvatura semelhante ao alvéolo, a qual poderá afetar o comportamento celular quando comparada com uma superfície plana.

Posto isto, o objectivo deste projecto é investigar a influência da curvatura em células epiteliais de pulmão humano cultivadas em substratos que contêm cavidades formadas por *microthermoforming*, as quais poderão ser modificadas por *ion track etching* para introdução de poros. Existem vários métodos de produzir cavidades em substratos poliméricos, mas o *microthermoforming* assistido por gás para além de permitir que as estruturas sejam da ordem dos micrómeteros com espessuras bastante finas, também admite que a sua replicação seja possível. Para além disso, esta técnica permite manter modificações prévias do material, como, por exemplo, irradiação com partículas pesadas energéticas, pois, durante o seu processamento, o polímero não é derretido. O policarbonato foi o material escolhido para suporte de cultura celular por ser biocompatível para a aplicação a que se destina e por ter óptimas propriedades mecânicas e térmicas.

De forma a alcançar uma estrutura para a cavidade o mais semelhante possível ao alvéolo humano, foram testados diferentes parâmetros para optimização do *microthermoforming* assistido por gás e do *ion track etching*. A avaliação do impacto que a curvatura poderá ter em células epiteliais de pulmão baseou-se na análise de resultados obtidos para proliferação celular, apoptose, densidade celular, adesão célula-substrato, interação célula-célula e teste de actividade metabólica. A caracterização destes resultados foi efetuada por marcação de estruturas específicas com anticorpos, microscópio electrónico de varrimento (MEV) e por microscopia laser de varrimento (3D perfilómetro).

O primeiro resultado positivo para implementação desta nova geometria em modelos alveolares foi a capacidade das células cultivadas em cavidades formarem uma monocamada celular confluente constituída por várias *tight junctions*, indicando a sua coesão. As membranas com cavidades mostraram um densidade celular (número de células por área) superior relativamente à mesma situação numa membrana plana. Para além disto, foi mostrado que uma célula individual em membranas com cavidades era rodeada por número mais elevado de células vizinhas devido aos ângulos adaptados forçados pela curvatura. Também uma primeira tentativa de criar uma interface ar-líquido foi experimentada para avaliar a integridade da barreira celular formada e o nível de diferenciação das células epiteliais, como assistida a nível alveolar. Uma camada celular confluente e coesa caracterizada pela existência de *tight junctions* foi alcançada e inúmeras células produtoras de muco foram observadas. O facto de o interface ar-líquido não estar optimizado e de ser impossível garantir que todas as células estariam expostas ao ar culminaram em resultados cujas diferenças óbvias induzidas pelo impacto da curvatura não foram encontradas.

Uma futura implementação de estruturas com curvatura em sistemas de microfluídica para modelos de pulmão mais realistas exige uma optimização dos resultados alcançados neste trabalho, os quais são bastante preliminares.

Palavras-chave: Pulmão, *in vitro*, modelo de linha celular, CALU-3, curvatura, policarbonato, *microthermoforming*, *ion track etching*.

Abstract

Tissue engineering aims to create functional tissues and *in vitro* biological structures using different technologies, approaches and to address different goals. An important strategy to have a better understanding of human organs and their interactions is by developing *in vitro* models that represent their anatomy and physiology.

In the particular case of this thesis, in order to mimic the human alveoli on a 3D *in vitro* model, efforts have to be made to develop a structure which shape and dimension are as close as possible to the native one in the human body (around 100μm in depth and 200μm in diameter [1][2][3]). Human lung *in vitro* models have been developed and improved for the past years, upgrading from two dimensional (2 D) models to three dimensional (3 D) conformation, such as lung organoids[4], but none in literature displays curvature in their platforms, which is believed to affect cells' behaviour.

Thus, the aim of this work was to investigate the influence of curvature on human lung epithelial cells on curved platforms created by thermoforming and modified via ion track etching. There are several technologies that enable fabrication of curved structures but gas-assisted microthermoforming allows the creation and replication of really thin walled microcavities, preserving any pre-modification of the used polymer such as irradiation with energetic heavy particles. Polycarbonate was the chosen material mainly because of its biocompatibility, mechanical and thermal characteristics.

Different parameters were tested to optimise gas-assisted microthermoforming and ion track etching in order to achieve a structure that was as close as possible to the human alveoli' dimensions and shape. To assess the impact of substrate's curvature on epithelial cells, proliferation, apoptosis, cell density, cell-substrate adhesion, cell-cell interaction and metabolic activity assays were performed. Samples were analysed and characterised by specific immunostainings by respective fluorescent imaging, by scanning electron microscope (SEM) and by laser scanning microscope

profilometer.

Cells were successfully cultured inside cavities and formed a confluent cell monolayer showing well defined tight junctions, which was the first positive indication about implementing a new geometry in these alveolar models. Cell density (more specifically, number of cells per area) was shown to be higher on curved substrates when compared to the same situation on a 2D flat membrane, where one single cell was surrounded by more cells enhancing cell-cell interaction in different angles. Furthermore, the first trial of an air-liquid interface culture was conducted to evaluate cell barrier integrity and epithelial cells' differentiation when exposed to air in a curved platform. A confluent cell layer was achieved, characterised strongly packed tight junctions and several mucous cells were observed. No obvious differences were noticeable regarding curvature impact and air exposure, mainly because the setup is still not optimal and it was not possible to ensure that cells were in fact exposed to air in all areas of the sample.

The continuation of this work and optimisation of preliminary results are imperative to a future implementation of curvature on a microfluidic system, aiming for a more realistic lung-on-chip model.

Keywords: lung, *in vitro*, cell line model, CALU-3, curvature, polycarbonate, microthermoforming, ion track etching.

Acronyms

2 D two dimensional.
3 D three dimensional.
ALI Air-Liquid Interface.
ATII Alveolar Type II.
ATI Alveolar Type I.
COPD chronic obstructive pulmonary disease.
DMSO Dimethyl Sulfoxide.
ECM Extracellular Matrix.
EDF extended depth of focus.
EMEM Eagle's Minimum Essential Medium.
EtOH ethanol.
FBS Fetal Bovine Serum.
HMDS hexamethyldisilazane.
HPAEC Human Pulmonary Alveolar Epithelial Cells.
MW molecular weighted.
PBS Dulbecco's Phosphate-Buffered Saline.
PC Polycarbonate.
PFA paraformaldehyde.
SD Standard Deviation.
SEM Scanning Electron Microscope.
TEER transepithelial electrical resistance.
TE Track Etch.
TJs Tight Junctions.

List of Symbols

μ**g** (μg) non-SI unit of mass.
μ**L** (μL) non-SI unit of volume.
μ**m** (μm) non-SI unit of length.

List of Figures

List of Tables

Contents

1

Introduction

1.1 Motivation

Despite all lung's defence mechanisms against harmful substances such as allergens, tobacco's smoke and chemical irritant particles, lungs' direct interaction with the increasingly polluted environment makes them an easy target for the development of anomalies [7], adding to the already possibly existent genetic problems.

Chronic respiratory diseases such as asthma, chronic obstructive pulmonary disease (COPD), chronic bronchitis and emphysema, affect one out of twelve humans in the world [8], generating an enormous public health burden [9]. These chronic inflammatory illnesses often result in obstruction of the airways and, consequentially, alveolar tissue destruction, affecting oxygen exchange [8]. Additionally, the fact that 20-35% of the world population smokes [8] and the environment is getting more and more polluted rises the amount of allergens affecting people, which in return help triggering well known dysfunctions in the airway epithelium[8].

An important strategy to understand and find better treatment approaches to these respiratory system's diseases is via study models which can be either *in vivo* or in *in vitro* platforms.

Even though *in vivo* animal lung disease models exist, they do not fully mimic the complexity of hemostasis and hemodynamic alterations of the human lung [10], having immune responses often due to unsuitable host. Furthermore, *in vivo* studies are time consuming, expensive [11] and raises ethical concerns which play a major role in this subject. In contrast, *in vitro* models allow faster results with smaller budgets. Albeit these models face bigger challenges to mimic the conditions of living organism, engineering and manipulation of its design enables the fabrication of the best platform possible. As an example, some *in vitro* disease models enable single analysis of multi-layered disease mechanisms when associated with complex mixtures

like cigarette smoke, allergen extracts or specific chemicals or proteins and can be used to assess the contribution of each cellular component for disease pathogenesis, showing a big advantage when compared to patient studies and *in vivo* models [8].

Mechanical and chemical environment present in these cell culture platform play an interesting role when trying to recreate an organ/structures *in vitro*. Regarding mechanical cues, although hard and soft materials had already been patterned in 2 D cultures [12], conventional 2 D models lack on specific spatio-temporal stimuli that influences cells to develop specific morphologies, their gene expression and cell cycle state. In contrast, it was proven that 3 D cultures in customised structures achieve closer cellular and tissue behaviours to their native state [13][12].

Cells and tissues in the human body are subjected to external forces originated from several sources such fluid shear stress, osmotic forces, mechanical load or stretch, as it happens in the lung [14] that play an important role when conjugated with geometry in guiding cell's function, shape, differentiation, cytoskeletal tension, polarisation and cell-cell communication. Furthermore, it was shown that Extracellular Matrix (ECM)'s signals [12] and stiffness [14] has a major influence, on regulating progenitor cells' function and fate *in vivo* [12]. This cellular conversion of a mechanical input onto an intracellular signal is known as mechano-transduction [14]. In a more specific note, past studies already showed that geometry might regulate temporally lung epithelial cells' function and its fate *in vitro* [12].

Nonetheless, introducing three-dimensionality via curved geometries in an organ *in vitro* model seems essential to closely mimic the native environment.

The motivation of this project rests in the few resources for realistic modelling and drug screening for lung diseases [15] developed and published in literature, that are all based in 2 D substrates which do not represent, at all, the human lung's anatomy. Introducing a more realistic geometry with curved porous substrates arranged in a similar manner to the human alveoli arrangement is imperative to create a more reliable and realistic *in vitro* model. In this thesis a curved bioinspired membrane will be engineered and incorporated into cell culture platform which will enable the study of how lung epithelial cells respond to curvature. This study is the first step towards the creation of a future "lung on a chip". Once achieved this platform will be implemented in a microfluidic system, where, both healthy and pathological states can be recreated. Besides a better understanding of the normal alveolar cell barrier's integrity and its proprieties, it will also be possible to assess human lung's pathophysiology. The study of lung's inflammatory responses and pre-clinical drug's administration evaluations will be possible by exposing this model to different

substances and conditions. These results will provide valuable information and the necessary tools for pharmaceutical and toxicological research, complementing or even replacing completely animal studies [9] [15].

1.2 State of the Art

Lung *in vitro* models, both 2 D and 3 D, have been used to recreate main cellular functions and, therefore, understand specific tissues, in terms of pathological changes and drug toxicity responses [16]. Some examples can be the development of alveolar-like tissue structures where surfactant was produced [17], pulmonary-alveolar-capillary barrier models [18] and cocultures of human bronchial cells and bone marrow mesenchymal stem cells under exposed to air to differentiate mucus producing cells [19].

The urge to solve some critical limitations associated with 2 D *in vitro* models', such as the inability to guide cells into ordered and hierarchical structures found in the human body [20] led to the development of 3 D *in vitro* models. Furthermore, the necessity of creating a controlled microenvironment where a simple *in vitro* 3 D cell model could be incorporated, exposed to different variables and monitored, culminated in the concept of "organ-on-chip" [20].

Organs-on-chips are miniaturised biomimetic microsystems with relatively simple designs, implemented in microfluidic systems with hollow microcompartments for cell culture. These models allow recapitulating organ function through mimicking the native's microenvironment and its basic physiological functions [10]. It's important to emphasise that the focus is not mimicking the organ's anatomy, since they are usually based on simple layers of specific cells in perfused microfluidic systems. Organs-on-chip might be useful for screening of cellular responses to different stimuli such as drugs chemicals, toxins or pathogens [11]. Imaging techniques and sensor for real-time readouts can be incorporated. The better the replication of the desired tissue's behaviour, the more reliable and predictive are the models' resulting information [21].

Even though single organ-on-chip are already complex to recreate, it was shown imperative to upgrade them to multiple-organ-chips. This concept conjugates physically separated tissues *in vivo* that depend on each other to properly function [22], recreating their interactions with an increased complexity.

The final goal is to create a "human-on-a-chip" model where different microengi-

neered components can interact and mimic what happens in reality. In order to accomplish this, different organ units have to be combined. Recently individual developments have already been improved such as human skin [23], gut [24], bone morrow [25][26], the liver [27], microfluidic models of kidney's epithelium [28], microfluidic 3 D blood-brain barrier models [21] and lung [15][9][10][11]. It is important to keep in mind that this extreme idea is far from happening, but this might be the future link between pre-clinical and clinical studies [22].

Focusing on the lung, back in 2010, the first lung-on-chip was published as a multifunctional microdevice representing the human alveolar-capillary interface, developed as a microfluidic chip based on a 10 μm thin, porous, flexible flat membrane coated with ECM (fibronectin or collagen) separating two parallel rectangular microchannels. This model reproduced complex inflammatory responses to bacteria and cytokines, close to organ-level [11]. In 2011, the previously used lung tumor cells A549 were replaced by primary human lung alveolar epithelial cells and human vascular endothelial cells that could line the microchannels and could be perfused by human blood instead of culture medium [10]. Under controlled conditions, this primary human lung alveoli chip could be perfused with whole human blood without producing thrombus, enabling real time analysis with high resolution of different human cells and human tissues such as the blood cells and the endothelial cells [10]. In 2012, a human lung disease was modelled, evolving from the previous lung-on-chip by mimicking pulmonary edema [29]. Three years later, COPD and asthma were modelled on a chip for drug screening, infection and exacerbation studies and a general better understanding on the subject [8][9]. Last developments in the organ-on-a-chip field focusing on the human lung are from 2017, where the airway epithelium in a microfluidic system is associated with electrodes to continuously monitor the formation and disruption of the epithelial cell monolayer and asses about the epithelial barrier function [15][30]. Most of these studies focus on epithelial exposure to a single microbial species, even though the airways also contain bacteria, viruses and fungi that affect the inflammatory response against inhaled pathogens as well [8].

In this thesis, a new approach will be presented of an microengineered human alveolar membrane. To the best of our knowledge, all lung models use flat 2 D membranes which do not represent, at all, the alveoli's structure. In order to investigate if microanatomy plays an important role when recapitulating lung's physiology, spherical microcavity with similar shapes to the human alveoli will be formed in thin polycarbonate dense and porous membranes. This curved platform will be lined by human epithelial lung cells and their response will be studied. The microthermoforming

technique used to create the cavities on the polycarbonate membrane allows the maintenance of possible pre and post modification phenomenons, such as cell adhesion micropatterns [31], previous heavy ion irradiation and ion track etched pores, as examples.

1.3 The Lung

The lung is a complex organ, not only anatomically but also physiologically and histologically [32], which development allowed vertebrates to live on earth [33]. Its main role is to exchange gases from the inhaled air to the blood and *vice versa*, in order to provide the necessary oxygen to the cells of the organism and to remove carbon dioxide from their metabolism's products [32][3]. Since the process of respiration is dependent on lung's structure [33], its overall properties are unique in order to achieve the maximum efficiency of this essential process [32]. At a functional level, three big phenomena happen in the lung: ventilation, circulation and diffusion which consist, in overall, of the oxygen conduction to the blood pulmonary system and of the carbon dioxide removal in the alveolus-capillary membrane [34].

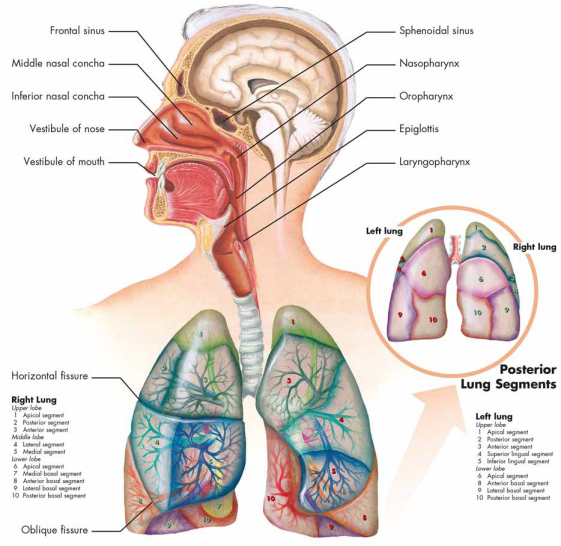

Figure 1.1: Anatomical representation of the human respiratory system. [Adapted from: 3B Scientific, item no: VR1322UU [4006675] - "The Respiratory System Chart"]

In the specific case of the human adult lung, there are around 300 millions of alveoli with a total surface area of approximately 140 m^2, comprising more than 99% of the internal surface area of the lung [1][3]. For the normal adult human alveolus, its main dimensions are around 250 μm in width and 100 μm in depth [2][3].

Briefly, the main anatomical structure of the respiratory tract consists of the large airways, the conducting portion, from the nasal cavity [34] to the tracheobronchial airway tree [32]) and the small airways, the respiratory portion, composed by the respiratory bronchioles, alveolar ducts, alveolar sacs and the alveoli. Responsible for ventilation are the rib cage, intercostal muscles, diaphragm and elastic fibbers from the conjunctive tissue of the lung [3]. The majority of the protective functions, such as warming and humidification of the inhaled air to the body, happens in the aerial transit section [32][34]. The small airways have seven levels of ramification, which structures have diameters under two millimetres, including the respiratory bronchioles, alveolar canals and alveolar cavities [34].

The tracheobronchial airway tree has a characteristic geometric structure to facilitate the direction of air to the gas-exchange region [32] and it is divided into the trachea, the bronchi and the bronchioles [35]. This branched structure regulates the gas flow and conditions the inhaled air [35].

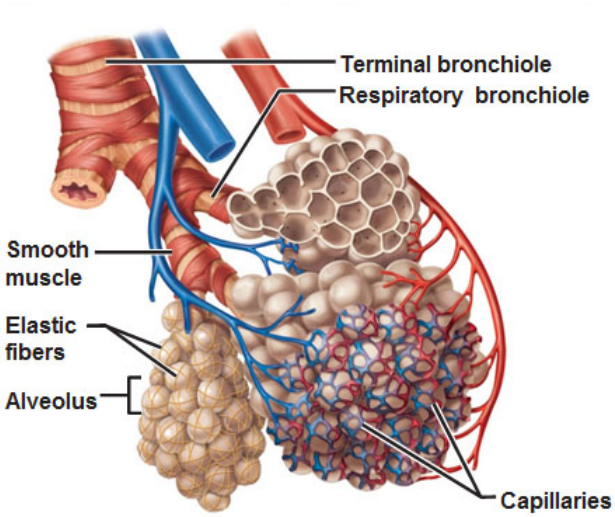

Figure 1.2: Diagrammatic representation of the capillary-alveoli interaction for the oxygen and carbon dioxide exchange. [Adapted from: www.antranik.org/the-respiratory-system]

The bronchioles establish the transition from the exclusively conducting portion to the respiratory area [3]. They continue to the alveolar ducts, cylindrical channels that open into the alveoli, small air bags encompassed by a huge capillary bed. The alveolus is the most specialised structure in the lung and it's responsible for the already referred major important function of gas-exchange [36]. They are organised into groups to facilitate the air delivery and distribution, and surrounded by a large capillary bed, where all cardiac output of venous blood from the right side of the

heart is received in each contraction [32]. The diffusion of gases happens through a tissue limited in thickness to facilitate this exchange known as the air-blood barrier [32].

The airways and the alveolar regions are lined with different kinds of epithelial cells which are essential in terms of physiologic function and, therefore, the starting point for the development of respiratory diseases [1][33]. Epithelial cells can be specified regarding their shape: pyramidal, columnar (height bigger than with), cuboidal (equal height and width), squamous (height smaller than width) and bottle cells (width at the cell centre is greater than at the luminal or abluminal ends) [35].

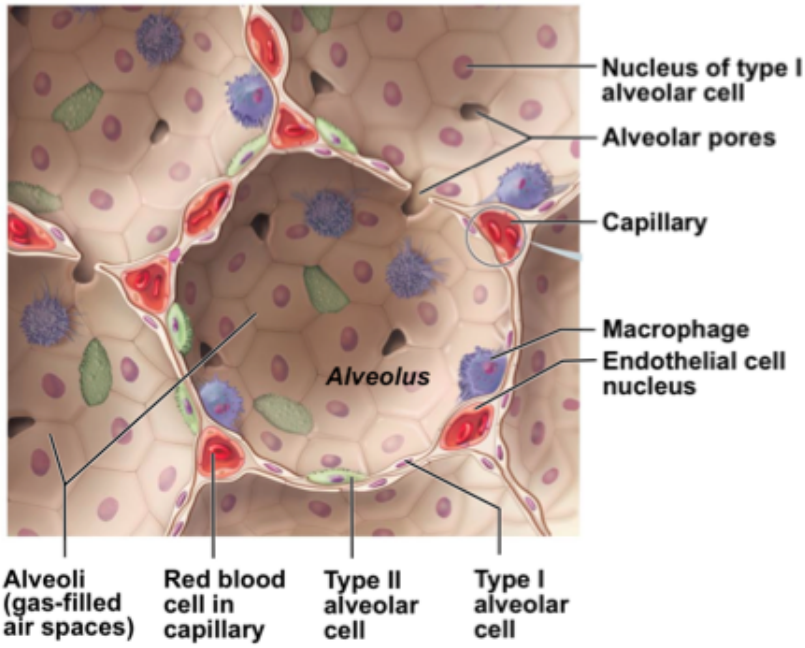

Figure 1.3: The respiratory membrane's diagrammatic representation. Macrophages, endothelial cells, red blood cells, alveolar capillary, alveolar pores and type I and type II alveolar cells are represented. [Adapted from: http://antranik.org/the-respiratory-system on July 15th 2017]

The conducting airways are mainly lined by a pseudostratified epithelium [33] (all epithelial cells have direct contact with the basement membrane although its nuclei forms two or more rows [35]) composed of several different surface epithelial cell types, mainly ciliated, basal, and and non-ciliated cells [33] with the main functions of secretion of mucus, ions, proteins, lipids, inflammatory mediators and participation in wound repair after injury, among others [37]. Since the airway epithelium is exposed to the external environment, it suffers diverse biophysical and biological stimuli resulting from the direct contact with exogenous substances, stress and medical drugs that work both as therapy and injury's factors [38].

Focusing on the alveoli, they are composed of simple epithelium, which consists in a single row of cells all in contact with the basement membrane [3]. There are two cell types lining its surface, the squamous ATI cell (pneumocytes I), making 8% of the total cells in the lung and 95% of the cells in the alveolar surface [1][3], and the cuboidal ATII cell (pneumocytes II), making 15% of the total cells in the lung and covering the last 3-5% available space in the alveolar surface [1].

Regarding their shape and dimensions, ATI squamous cells are flat (height of 25-100 nm) and bigger, with a diameter between 50 and 100 μm. These large areas of attenuated cytoplasm facilitates the gas exchange once the diffusion is across a thinner barrier [37]. In contrast, the ATII cells are smaller (diameter around 10 μm), cuboidal and exhibit crucial functions such as the production, secretion and recycling of pulmonary surfactant [1] (a mixture of phospholipids and proteins that lowers the surface tension in the air-liquid alveolar interface [37]) and actively transport of ions [1], granting them a relative bigger metabolic activity [37]. Furthermore, besides including microvilli and secretory granules [37], *in vivo*, they are progenitor cells and respond to lung's injury by proliferating [1]. In the interalveolar septo there are alveolar macrophages which can migrate to the alveolar sac, adhering to the epithelial cells and phagocytasing bacteria and other inhaled particles [3].

Gas-exchange happens across alveolar epithelial cells and capillary endothelial cells in such proximity that the basement membranes of both types of cells fuse, forming an extremely thin barrier of high surface area [33] [37]. Ventilation, on the other hand, depends on mechanical forces resulting from neuromuscular activity which is controlled by the pressure levels of carbon dioxide, oxygen and the pH. Injured lung cells rapidly spread and migrate to cover damaged epithelium but, in contrast, the proliferative rates in the mature lung is relatively low, having a cell turnover of many months when no injury happens [33].

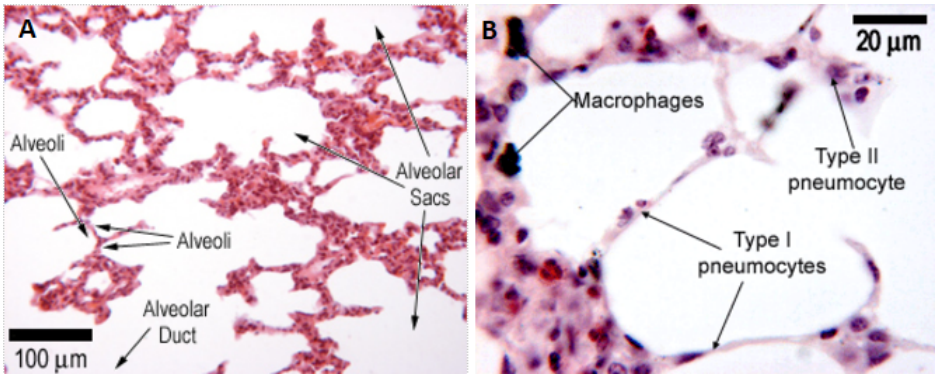

Figure 1.4: The alveolar region histological cross section. On the left image (A) alveolar sacs, alveolar ducts and alveoli are represented. On image (B) macrophages, ATI and ATII are visible. [Adapted from: http://www.histology.leeds.ac.uk/respiratory/respiratory.php on September 9th 2017]

1.4 Cell Culturing

The first epithelial cell culture was in 1922, the HeLa cells, a continuous epithelial cell line, even though it was only reported in 1953. The first statement of the usage of a lung cancer epithelial cell line was in 1955, followed by the growth of cells from normal human bronchus explants, three years later [1].

1.4.1 The importance of 3 dimensionality

In the human body, almost all tissues are settled in an extra cellular matrix composed by a 3 D complex of a fibrous mesh-work [39] but for many years, *in vitro* studies have been performed on 2 D flat surfaces [40] such as micro-well plates and tissue culture flasks. From a material's perspective, these surfaces are simple, cheaper to fabricate and widely commercially available. From a biological approach, they are easy to use and generally result in high cell viability [39].

The conventional 2 D cell culture models were thought to provide a good understanding of the cellular physiology, however, there are strong evidences that this is not entirely true. Back in 1997, human breast cancer models where shown to be more successful when improving to 3 D, when comparing to the previous 2 D models [41]. In 2002 it was showed that cues from cell adhesion to ECM and neighbour cells interaction regulates cells' behaviour, coming up with the necessity to engineer more *in vivo*-like structures instead of 2 D platforms [42]. In 2005, it was proved that cells

grown in 2 D *in vitro* models are perturbed by the microenvironment, expressing different genes compared to their expression in the origin tissue [43].

Transitioning from 2 D cell cultures to 3 D cell cultures [44] (scaffolds, porous substrates where cells' growth, organisation and differentiation is supported [39]) introduced new essential scientific knowledge and new insights on cell behaviour understanding like proliferation, differentiation, adhesion, viability, morphology, angiogenesis and immune response [44]. A microengineered 3 D cell culture is a microfabricated device with 3 D structures where living cells are cultured and maintained in order to mimic tissue and organ specific architectures in a microscale [45]. The major advantaged of this upgrade is the recovery of very important information concerning cell-to-cell and cell-to-matrix interaction, once lost in the conventional method [40]. Besides 3 D models having an incredible homogeneous cell study material for research, cells also adapt the right behaviour, closer to what happens in real conditions, providing a better understanding in complex interactions and leading to more advanced equipment and techniques [40]. One of the major advantages is that in a 3D context, complex tissue's differentiation occurs naturally, which can be very useful for human stem cells, where human material can be differentiated into cells of interested and, consequently, create human tissue *in vitro* [46]. Furthermore, due to cells interaction in 3 D platforms being more approximated from their behaviour *in vivo*, they are thought to provide more accurate results and, therefore, a better prediction for clinical outcomes [47]. In 2014, this approach was used in more than 380 different cell lines [40]. One important factor to keep in mind is that the quality of the used model is specific for the cell line and project's goals and has to be analysed once they can or cannot represent the true behaviour of the cells *in vivo*, resulting in a not so reliable data acquisition [46]. Some of the most popular three dimensional cell culture examples used nowadays are aggregate cultures, spheroids, hydrogels and scaffold-based technologies [46], which have several biological applications, such as pharmaceutical studies and increasing drug discovery efficiency, cancer research, studies in gene and protein expression and tissue engineering and the understanding of cell physiology, facilitating cell-substrate adhesion studies, which is one of the concerns in this project [40].

1.4.2 Cell barrier formation

In order to efficiently seed cells on a substrate, meaning that they adhere, migrate, proliferate and differentiate without losing their characteristics or dying, the material has to be functionalised to acquire spatiotemporal patterns of chemical and

biophysical cues, vital for the needed microenvironment [48].

In vivo, cell adhesion results from extrinsic factors of the extra cellular matrix such as integrin ligands [48] making a good bridge to possible solution for *in vitro* models. However, besides the hydrophilic preferred properties of a polymer, several other material modifications like coatings and micro/nanopatterns increase the chances of controlling the adhesion to the material, highly affecting the cell-fate [44]. Deep ultraviolet treatment, incorporating ECM components such as collagen, fibronectin or laminin and hydrophilizating the polymer are some of the methods to functionalise the surface the interested material, providing a proper biochemical microenvironment to the cells. Manipulating these elements and their quantities helps finding the needed balance between cell adhesion on the cavity surface and cell aggregation inside its volume [44].

Cell Tight Junctions (TJs) can be described as a continuous circumferential seal around cells formed by several filaments of fibrils that can be localised by four integral membrane proteins such as occludins, junctional adhesion molecule, claudins and the coxsackie and adenoviral serotype 2/5 receptor. It separates the apical and basolateral compartments of epithelium [49]. Focusing on the occludins, they regulate diffusion of hydrophilic tracers of small size and neutrophil transmigration. TJ's main role is limiting paracellular permeability to ions and solutes, adapting a gate and fence function towards them, lipids and proteins diffusion and maintaining the epithelial homeostasis [49].

To successfully achieve a "organ-on-chip" it is essential to have these basic culturing concepts of the cell-cell interaction (TJs) and cell-material interaction (adhesion). This is the first step to understand how a 3 D microfluidic model can function and simulate a living organ and design the most appropriate and advantageous *in vitro* system.

These basic cell-cell and cell-substrate characteristic bonds established are essential for an successful cell culture in 3 D substrates and for the resulting cell barrier formed.

1.5 Curvature in cell culture platforms

Several methods have been applied to shape polymers, either by primary forming processes such as micro injection moulding, injection compression moulding and hot embossing, where the polymer is melted, or by secondary forming processes such

as blow moulding and thermoforming, where the polymer is in a solid but softened thermoelastic state [5]. In most cases materials suffer a pre-modification before shaping, which is only preserved if the moulding process doesn't melt the polymer. For that reason, secondary forming processes can be advantageous for lab on a chip's applications [5].

Even though blow moulding has been used to produce some medical balloons for miniature angioplasty, vessel occluding and artery perfusion, it has been shown difficult to produce layouts of chips due to the produced dimensions of the final material's parts [5]. Regarding hot embossing, also known as thermal imprinting [50], even though it is very similar to microthermoforming by using the polymer in the same initial state and by heating it up above its glass temperature with hot presses, the final products are distinct. In hot embossing the polymer fills the total volume of compact mould regions and for that reason, the thickness of the initial material film has to be bigger than the depths of the mould structures and the final product cannot be a thin-walled hollow structure. On the contrary, gas-assisted microthermoforming uses free forming concepts where depending on the used pressure, the heated up and softened material stretches to adapt to the available spatial shape of the mould [5]. Microfabrication of "organ-on-chip" devices with advantageous characteristics for its implementation in tissue engineering requires well thought and specific fabrication methods that allow its reliable production [5]. For that reason, microthermoforming has been rising, for the last ten years, as a polymer moulding technique to produce really thin walled polymer microstructures [5]. Microthermoforming technology has already been applied in several microfluidic products, cell chips and microchips for cell culturing and artificial *in vitro* capillary network, among others [5].

1.5.1 Gas-assisted microthermoforming

Gas-assisted microthermoforming is a technique in which a semi-finished product is heated (and, therefore, softened) as a thermoplastic polymer film or plate, keeping its edges fixed, in order to confer it the desirable shape of a mould by three-dimensional stretching [5]. The polymer film must be a thermoformable material [51] which means that it has to achieve an elastic state so that it can be stretched to adapt the mould's shape without tearing apart. This phenomenon happens when the material is put in a temperature condition above its glass temperature and bellow its viscous state [5]. Firstly, the polymer film has to be heated up which can be done by contact, convection or radiant heaters depending on the chosen thermoforming

technique. The shapinge, the moment when the polymer bends around and lines the inner surface of the mould, is performed either by mechanical tools, vacuum or compressed air ("pressure forming") [5].

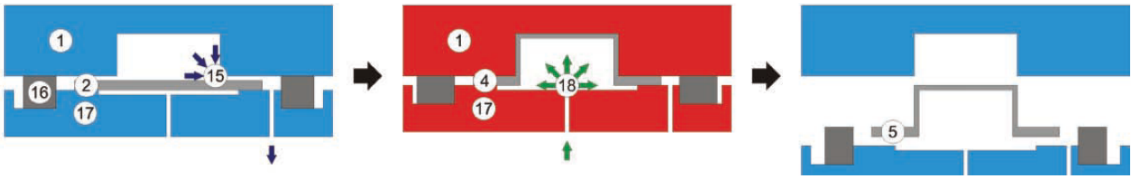

Figure 1.5: Simplified scheme of microthermoforming with compressed gas-micro pressure forming with a "negative" mould formation. (1) micromould, (2) thin thermoplastic film, (4) softened and formed film, (5) solidified thermoformed film, (15) vacuum, (16) axial seal, (17) counter plate with openings for evacuation and gas pressurisation, (18) compressed nitrogen; blue represents cold parts and and red heated[5]. [Adapted from: "Thermoforming of Film-Based Biomedical Microdevices", Roman Truckenmüller, Stefan Giselbrecht, *et al.*].

Depending if the film is formed over the protrusions of a mould ("positive") or into empty depressions of a mould ("negative"), the inner surface of the thermoformed material replicates the desired shape or the outer part of the thermoformed polymer replicates it, respectively. After applying the necessary temperature and stretching method, the film is cooled down below the softening temperature in order to keep the new three-dimensional structure. Some of the advantages of using this technique are the preservation of the structure and properties of textured, printed or multilayer films after processing, the fabrication of thin-walled pieces, the relatively low tooling costs and short interval time from design to production of the product [5].

1.5.1.1 Polycarbonate Membranes

The developments and advances in tissue engineering increased the potential usage of synthetic polymers that gather demanding requirements for different biological applications, which has been the focus of several researches for *in vitro* models [52].

PC are thermoplastics that show a set of unique characteristics when compared to the other polymers previously referred [53]. Some examples are the good mechanical strength and toughness [52] [53], high transparency, dimensional stability for a wide temperature range (T_g=148^oC [54]), good electrical properties [53], very slow degradation rates *in vitro* and non-toxic products of degradation (carbon dioxide and two alcohols) [52][53]. The pendant group can vary as the final features of the polymer are required. In previous studies, for example, using polycarbonate with

an ethyl ester as the pendant group provides strong osteoconductive proprieties, sufficient mechanical properties for load bearing for bone fixations and promotes significant bone growth [52]; poly(BPA-carbonate) is extremely stable and virtually non degradable in physiological conditions; tyrosine-derived polycarbonates showed good interaction with canine bone and no fibrous layer was formed around it as a immunoresponse, putting them as a strong candidate for tissue engineering scaffolds [55]. Due to all these characteristics, PC was the election polymer making it possible to choose from several microprocessing methods to achieve the wanted curved shape [56].

1.5.2 Ion Track Etching

Ion track etching is a technique used to produce pores, as an example, in a polymer, by irradiating it first with swift heavy ions [57] (either fragments from the fission of heavy nuclei or ion beams from accelerators [58]), followed by a chemical etching of the formed latent tracks [57]. The etching solution is alkaline and it may contain a surfactant that significantly influences the shape of the pores once the molecules may adsorb on the polymer surface and alter its susceptibility to the chemical attack [59]. Many geometries can be achieved for the pores, with different diameters ranging from the nanometre scale to tens of micrometers, depending on the polymer's chemical structure, the prior irradiation of it and the etching parameters used [57]. The bulk etch rate is dependent on the composition of the etchant solution, on the material composition and structure and on the etching temperature. On the other hand, the track etch rate is more complex and it depends on several other factors such as the sensitivity of the material, the irradiation and post-irradiation conditions and on the etching conditions [58]. The resulting Track Etch (TE) membranes are widely used for the synthesis of nanostructured and microstructured materials for porous systems' models, making it imperative to keep the pore size and its geometry controlled and constant [59]. Polymers such as polyethylene terephthalate, polycarbonate, polypropylene and polyimides are particularly used for the ion track technology [58].

In the specific case of polycarbonate immersed in an etching solution with surfactant, initially the polymer's surface is covered by the surfactant molecules, protecting it from the hydroxide ions' attack. Once these ions diffuse across the formed surfactant layer, the cleavage of the carbonate groups of the polymer's surface and track entries starts and the pores formation is initiated by creating small holes on the track entries. As the hole achieves a big enough diameter, the surfactant molecules penetrate the

formed hole's neck and start covering its wall, creating a layer as thick as the radius of the formed track. By this moment, only the hydroxide ions and cation's diffusion is allowed into the pore, creating a larger diameter under the hole's neck, where the surfactant layer is not created until molecules are able to pass again. At the same time, the bulk area of the polymer is etched as well, creating a further growth of the pore and a wear of the rest of the polycarbonate [59]. Due to its relatively high sensitivity, it is possible to produce pores with diameters around 0.01 μm. Polycarbonate track membranes have a relatively low resistance to organic solvents and relatively low wettability when compared to other etched polymers such as polyethylene terephthalate [58].

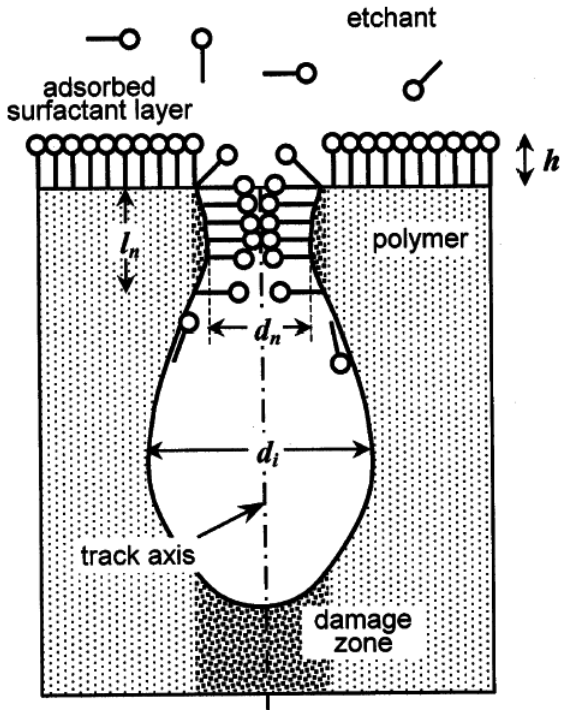

Figure 1.6: Representation of the initial stage of track etching phenomenon on a polymer by a nanosized surfactant molecule (the circular part is hydrophilic and the flat part hydrophobic).[Adapted from: "Structure of polycarbonate track-etch membranes: Origin of the "paradoxical" pore", P.Yu.Apel, *et al.*].

The polycarbonate track etched membranes were commercially available since the early 1970's, a few years after the particle track etching in thin films was discovered to produce porous membranes. The advances in this technological field were associated with the discovery of particle accelerators and the growth of new polymeric materials' knowledge such as new methods for its modification and further applications. Commercially produced track membranes usage can be separated in three groups: cell culture (porous membranes to seed cell and study their trans-

port, absorption and secretions activities), laboratory filtration (disks and filtration kits to collect small particles on the membrane surface for after analysis) and process filtration (purification of deionised water in microelectronics and separation and concentration of suspensions, for example), even though this last one has a big competition from casting membranes [58]. Hereupon, this technique may be advantageous for the fabrication of a a desirable structure for models of human organs with pores, such as the skin and the alveoli.

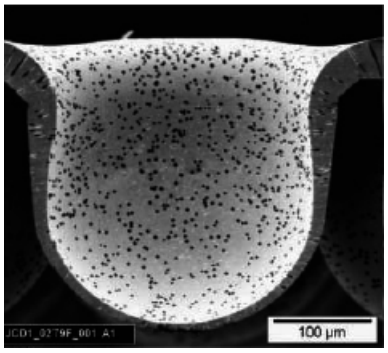

Figure 1.7: Cross sectional view of a SEM image from a track-etched polycarbonate microcontainer for cell culture using SMART technology [6]. [Adapted from: "3 D tissue culture substrates produced by microthermoforming of pre-processed polymer films", Stefan Giselbrecht, Roman Truckenmüller *et al.* [6]].

2

Materials and Methods

2.1 Polycarbonate Membranes

The chosen polymer for this study was a 25μm thick polycarbonate film previously irradiated with a heavy ion beam forming a pore density of 1×10^6 pores/cm^2 (ipPORE^{TM} Track Etched Membrane, *it4ip*: ion track technology, lot: M/080317/A/10 ref: 1000M25/610N000/A4).

2.1.1 Fabrication: Gas-Assisted Thermoforming

The main setup for gas-assisted thermoforming consists of a heating apparatus, a gas source and a previously designed mould, which is docked in between two brass plates with a PC membrane (partial setup on the left image from **figure 2.1**). For this model, the mould was composed of eight arrays of 9×9 cavities.

After conferring that all necessary cables were assembled, the chiller was turned on and the forming temperature was set the heating apparatus. While the temperature increased, the PC sheet would be cut and put over the mould. Both polymer and mould were put in between the two piece brass plates of the thermoforming machine, assembling these two parts to be perfectly docked together. The heating press was completely closed using a mechanical pressure valve. The forming process worked by Joule effect (contact heating) and after the selected temperature was achieved (higher than the glass temperature $T_g = 148^oC$ of polycarbonate), the gas pressure would be set on the digital pressure controller and applied. The applied gas, in this case nitrogen, forced the film into the holes of the mould around the softening temperature of the polymer [44]. After the process finished, the tool would be cooled down, the gas pressure would decrease and the thermoformed structure would be stable again [31]. Thermoforming parameters were optimised in order to achieve

cavities with 100 μm in depth. Each thermoforming session took around 40 minutes and the result was a PC membrane with 8 arrays of 81 cavities each.

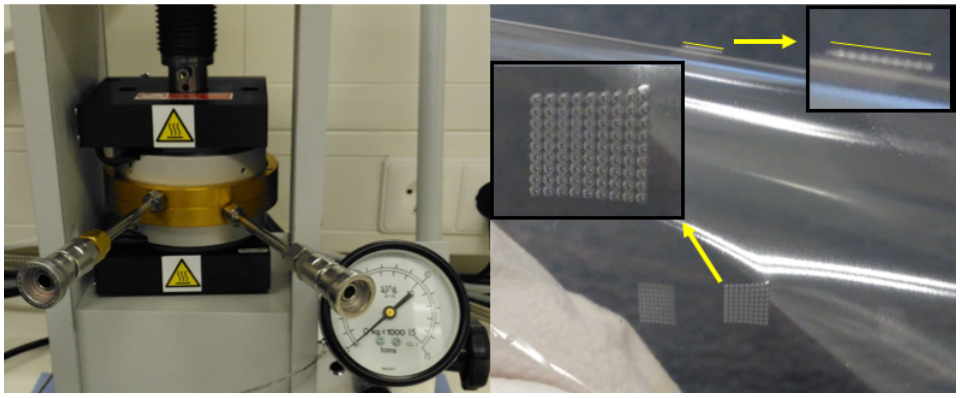

Figure 2.1: Part of the thermoforming machine set up: brass plates assembled with mould and PC film docked inside and mechanical pressure meter (left); Thermoformed PC membrane. Full cavities array and side view zoomed in (right).

2.1.1.1 Thermoforming Parameters Optimisation

Depth and shape of the cavities was one of the main concerns for the success of the project. A depth and shape as close as possible to the human alveoli's was required. For that matter, different forming temperatures (153^{o}C and 155^{o}C) and gas pressures (5 bar, 8 bar, 10 bar and 11 bar) were tested. Since it is the temperature that mainly affects the possible deformation of the material, this was the first to be selected. The lower option was chosen once it was enough to put the polycarbonate in a ductile state.

2.1.2 Film Modification: Ion Track Etching

As it was mentioned before, the original polymer film was dense and in order to make it porous it was carried out chemical etching and both thermoformed and non-thermoformed PC membranes were track etched to produce pores.

Firstly, the etching solution was prepared inside a laminar flow hood dissolving sodium hydroxide (NaOH) (VWR, serial: C00439 Cat:1.06462.1000) and pure methanol (Sigma-Aldrich, serial: C00509, Cat: 32213-2.5L-M) in distilled water. Since the reaction is highly exothermic, the NaOH had to be added slowly to make sure its pellets were completely dissolved and avoiding the solution to overheat. Ice was used to refrigerate the glass bottle containing the solution. Once prepared, the solution could be used or carefully stored for future experiments.

Once the etching's setup was assembled - hot place (IKA® C-MAG HS 7), thermometer (IKA®, ETS-D5), stainless steel rod and beaker), the etching solution was poured in, heated up to 70°C and the PC samples were placed in. After the previously mentioned temperature was achieved, the samples were submersed in the etching solution, the etching temperature would be set in the thermometer and maintained at 65°C. The duration of the process is dependent on the desired final pore size. Importantly, since water evaporates during the process, and it is crucial to keep the same concentration of the etching solution throughout the entire time, it was necessary to add more distilled water to compensate for it.

After the etching session, the samples were washed with water to stop the etching process faster and to remove as much etching solution as possible. Finally, the used solution had to be discarded and, therefore, neutralised with Chloridric Acid (HCl) that would be slowly added until the measurement with a pH indicator paper confirmed it to be neutral.

2.1.2.1 Etching Time Optimisation Curve

In order to assess the superficial diameter of the pores created in the PC membranes by this technique, triplicates of thermoformed (referred from now on as **"curved"**) and non thermoformed (**"flat"**) PC membranes were ion track etched for 1 hour, 2 hours, 2 hours and 30 minutes, 3 hours, 3 hours and 30 minutes, 4 hours, 4 hours and 30 minutes and 5 hours each, making a total of 24 curved and 24 flat samples. After each time point, samples were rinsed in water and let immersed for around 30 minutes.

One day after, when the samples were completely dry, it was measured the pore's superficial diameter with the profilometer optical microscope by using the diameter measurement tool from VK-X Series MultiFileAnalyzer. To finish, the data was analysed in Excel.

2.1.2.2 Etched PC's Thickness Variation Curve

For this measurement, it was used the profilometer as well, selecting the transparent film mode, 1 line (1024x1) area and analysing the resulting image in the VK-X Series Analyzer to determine the direct thickness.

In order to obtain the correction factor from the mechanical measurement and the optical and obtain the real value for thickness, five points were marked in a non

etched and non thermoformed PC membrane and thickness was measured using both laser scanning microscope profilometer and the mechanical probe (Heidenhain SG 60M, serial 48047807). Resulting data was analysed and processed in Excel.

2.1.3 Characterisation: Profilometer and SEM

2.1.3.1 Profilometer

Cavity's depth, shape, film's thickness and pore sizes were measured with the laser scanning microscope (profilomete keyence VK-X Series). For the depth, shape and pore size of the cavities, it was used the VK-X Series MultiFileAnalyzer while for the thickness measurement it was used the VK-X Series Analyzer.

For the depths determination correspondent to the forming pressures of 5 bar, 8 bar and 11 bar the laser microscope for 3 D and profile measurement (Keyence VK-X200 Series) was selected. After setting the upper and lower position of the cavity, the image was acquired in a surface profile mode, a standard (1024x768) area and processed in the VK-X Series MultiFileAnalyzer software. For the shape of the cavity the "Arc R" option was set while for the cavity's depth the bottom and the top of the cavity were determined with the "Max. Pt" option, a line was defined to pass on those 2 points and the vertical distance "Pt-Pt" was measured. All data was then processed and analysed in Excel (Microsoft Office, USA).

2.1.3.2 SEM

SEM (Scanning Electron Microscope FEI/Philips XL30) was used as an auxiliary tool to analyse and confirm the pore size of the etched membranes measured with the profilometer. For this matter, PC samples were mounted on top of the SEM's supports using a double sided carbon tape and gold sputtered (CRESSINGTON Sputter Coater/DOMPELAPPARAAT) for 100 seconds. An accelerating voltage of 10 kV and a working distance of 10 mm was used to acquire the images.

2.2 Cell Culture

2.2.1 HPAEC

Primary cells are derived from live tissue's biopsies and are commonly chosen as the biological material for organs-on-chip systems [22] since they represent many advantages for cell culturing such as their fast availability when compared to other cell type, by providing less batch-to-batch differences [21], introducing clinical relevance, less fluctuation in the results *in vitro* and for being easy to maintain in culture for weeks after isolation [22]. However, during the immortalisation process, they might loose part of their phenotype and genotype [21].

HPAEC can be acquired as type I, type II or a mix of both types regarding the aim of the study to be performed. Since they are primary cells from the alveoli they are supposed to differentiate and adapt to stimuli (shape, chemical, electrical or biological) received.

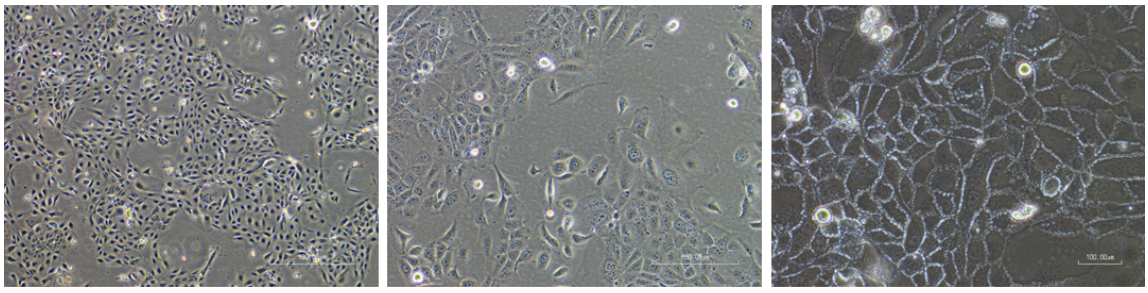

Figure 2.2: Morphology of HPAEC (passage 8) cultured in a 0.2% Gelatin-Based Coating Solution (PELOBiotech, PB-6950-100) Nunc^{TM} cell culture treated T-flask 75 (ThermoFisher Scientific). Inverted microscope (Nikon eclipse TS100) images, magnification: 4x, 10x and 20x, respectively. Scale bar: 100 μm

HPAEC was obtained from PELOBiotech (PB-H-6053) and kept in the liquid nitrogen tank in individual vials. Once thawed (medium refresh the day after to remove Dimethyl Sulfoxide (DMSO)), it was cultured in a 0,2% gelatin-based coating solution (PELOBiotech, PB-6950-100) coated T-flask 75 cm^2 (ThermoFisher Scientific^{TM}, Nunc^{TM} Cell Culture Treated EasYFlasks^{TM}) in an appropriate culture medium (Human Lung Epithelial Cell Growth Medium Kit classic: (PELOBiotech, PB-MH-350-3190) with a supplement kit (PELOBiotech, Cat. PB-MH-350-3190, Lot: QC-04B17F06) Fetal Bovine Serum (FBS) (65mL) and incubated at 37^{o}C, atmosphere of 95% air and 5% carbon dioxide. The medium was aliquoted in several 50mL falcon tubes to avoid possible contamination.

2.2.1.1 HPAEC Growth Curve

Ten treated 6-well plates for 10 different time points (VWR, Nunclon Delta, Serial B00177, Cat. 391-8036) were coated for 15 minutes with 0,2% gelatin-based coating. HPAEC were seeded in triplicated with two different cell densities of 1×10^4 cells/well and 1×10^5 cells/well set as "low density" and "high density", respectively. Each well had 2mL of culture medium for the cultured cells. Measurements were performed daily except the final well plate, which was counted 3 days after the last well plate's counting (13 days after HPAEC were cultured).

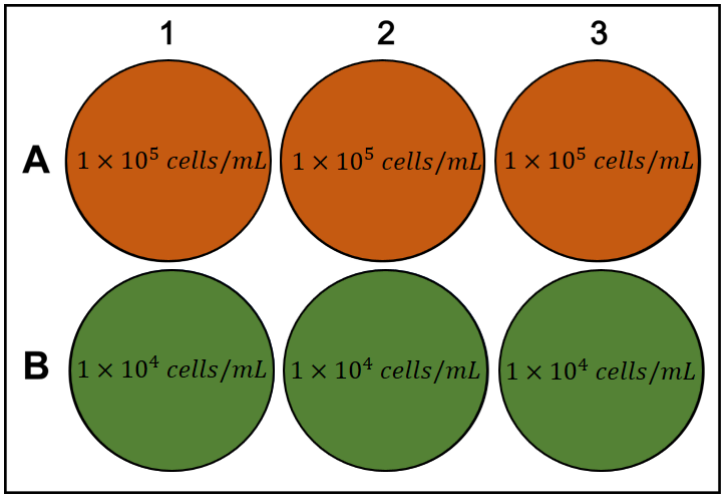

Figure 2.3: Representative template of the cell growth curve experiment for the HPAEC representing both "high" and "low" cell densities.

Everyday, all 6 wells of the considered time point were trypsinised and incubated for 6 minutes, neutralised with double the amount of culture medium and centrifuged (eppendorf, centrifuge 5810 R) for 5 minutes at 140 rcf, removing the supernatant afterwards and adding the necessary culture medium's volume. After, the number of cells in that volume was counted. In the first 5 days, mainly due to the well plates corresponding to the "low density" of HPAEC, cells were re-suspended in a smaller volume of 20μL of culture medium. For the following days, both cell densities were re-suspended in 100μL of culture medium. Daily images of the 6-well plates were taken as well to compare HPAEC's behaviour in culture with time.

2.2.2 CALU-3

CALU-3 belongs to the respiratory cell line group [60] derived from human bronchial submucosal glands [38], demonstrating several characteristics of bronchial epithelium

[61]. They are acquired from carcinogenic cell lines and show a good ability to form robust barriers [8], being one of the few with the capacity of forming strong tight junctions *in vitro* [60], to have a cellular responses to oxygen and ventilator induced lung injury, functional barrier of the bronchial epithelium and drug transporters [61], resulting in a set of unique features to represent a model of the airway epithelial barrier in the human lung [60]. Besides displaying microvilli, expressing the protein proSP-C specific for the lung surfactant and containing mucin granules, this cell line grows rapidly, consistently and can be reliably used after many passages [61]. However, culture conditions highly affect CALU-3 differentiation, expressing different cell structures if submerged in culture medium or exposed to air [61].

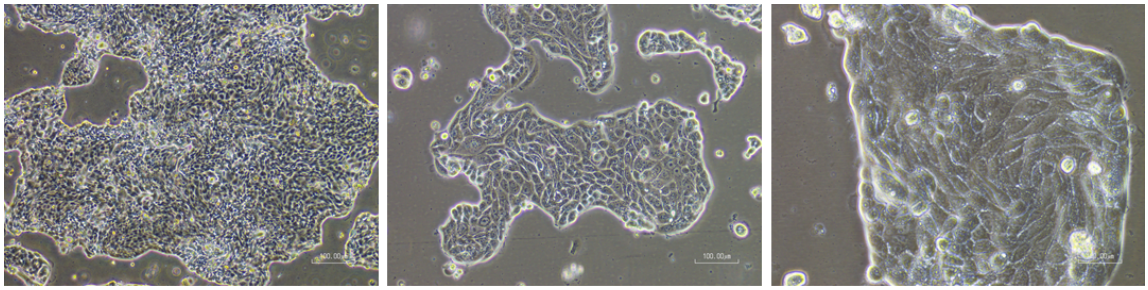

Figure 2.4: Morphology of calu-3 (passage 5) cultured in a Nunc^{TM} cell culture treated T-flask 75 (ThermoFisher Scientific). Inverted microscope (Nikon eclipse TS100) images, magnification: 4x, 10x and 20x, respectively. Scale bar: 100 μm

Human lung's adenocarcinoma cell line (CALU-3) was obtained from a 25 years old Caucasian male (LCG standards-ATCC, HTB-55) and kept preserved in the liquid nitrogen tank (CryoFill Solutions) in individual vials. Once carefully thawed, its medium was refreshed the day after to remove DMSO. CALU-3 were cultured in T-flasks of 25 cm^2 (Nunc^{TM} Cell Culture Treated EasYFlasks^{TM}, ThermoFisher Scientific^{TM}) in an appropriate culture medium of Eagle's Minimum Essential Medium (EMEM) from Lonza (Westburg, LO BE12-662F), supplemented with 6 mL L-Glutamine 200mM (Fisher Scientific, 11510626), 6 mL Pen/strep (Fisher Scientific, serial C00240, Cat.11548876), and 10% FBS (65mL) (Sigma-Aldrich, serial C00357,Cat. F7524-500mL), incubated at 37^{o}C, atmosphere of 95% air and 5% carbon dioxide. Culture medium was refreshed every 2 days until cells were 80% confluent. At this point, cells were trypsinised, counted and passed in a ratio of 1:2. For this matter, after removing the used medium, cell layer would be rinsed with Dulbecco's Phosphate-Buffered Saline (PBS) (Sigma-Aldrich, Cat. D8537-500ML, Lot. RNBG0543), 1 mL of trypsin/EDTA 0,05% (Fisher Scientific, Cat. 25300054, Serial C00333) would be added to the T-flask and put in the incubator for 6 minutes. Finally, the double volume of culture medium would be added to neutralised

the trypsin. For cell counting, 10 μL of cell suspension was mixed with 10 μL of trypan blue 0,4% (Sigma-Aldrich, serial C00359, Cat. T8154-100ml) and either counted manually in a Inverted Microscope (Nikon Eclipse TS100) or automatically in a Automated Cell Counter Machine (Bio Rad TC20^{TM}).

2.2.2.1 Curvature study: CALU-3 cultured on submerged dense membranes

Firstly, PC membranes were thermoformed for curved samples. A total of 32 circular samples (16 flat and 16 curved) were manually cut with a size 14 of the cutting tool from Mob Peddinghaus on the manual puncher Albert Klopfer GmbH (www.original-klopfer.de). Extra attention was needed when punching the thermoformed samples since it is advantageous that cavities' array are on the middle of the sample.

Then, samples were taken to the tissue culture laboratory and cleaned in a sterile environment by rinsing each one of them in a gradient of decreasing percentages of ethanol (EtOH) (100%,70%, 50%, 20% and distilled water twice) and mounted in four 24 treated well plates with black o-rings (Eriks, Cat. 12213774), inside the laminar flow hood. Each well plate corresponds to the a desired time point to keep cells in culture before fixing (24h, 48h, 72h and 11 days). Curved samples were placed inside the well plate with their bottom part facing up, so that cells could be cultured inside the cavities.

CALU-3 kept in culture in T-flasks 25 cm^2 were trypsinised and used at a passage 4 (P4). Cells were seeded with a density of 70 000 cells per well in a cell suspension drop of 50 μL and incubated for 3 hours. After the incubation time, 1mL of culture medium was carefully added and put back inside the incubator. Culture medium was refreshed every 2 days.

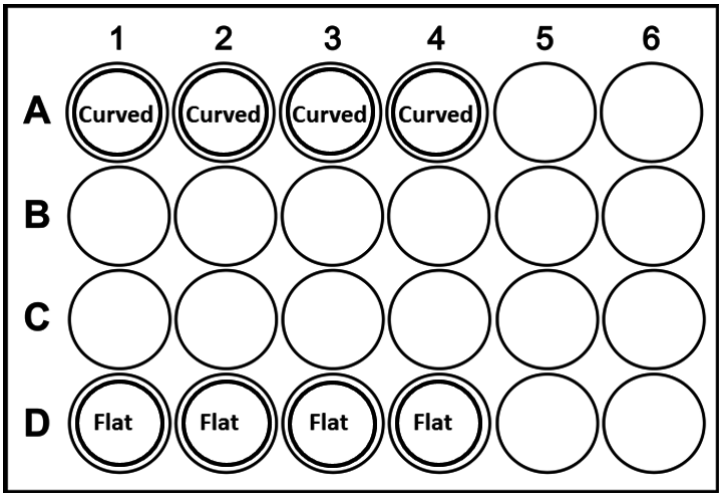

Figure 2.5: Representative template of curvature study's experiment display. 4 curved PC samples and 4 flat PC samples are fixated with a black o-ring and submerged in culture medium.

After each desired time point, cells were fixed. Culture medium was removed, cells were washed three times with PBS and 200 μL of 4% paraformaldehyde (PFA) was added for 30 minutes at room temperature. After the fixation time, cells were stored in PBS at 4^{o}C.

2.2.3 Immunofluorescence

Prior to the cells' staining, PBS (non sterile) and Triton X-100 0,1% were prepared. For the first, 500mL of distilled water was stirred with 5 pellets of PBS (VWR, Serial C00406, Cat. E404-100TABS) until completely homogeneous. Triton X-100 10% was achieved by diluting 2mL of Triton X-100 (VWR, Serial C00453, Cat. 437002A) 100% in 18mL of PBS and then diluted again by adding 0,5 μL of Triton X-100 10% to 49,5mL of PBS to obtain Triton X-100 0,1%.

Fixed samples in 4% PFA were submerged in Triton X-100 for 10 minutes to permeabilised the cells' membrane. After washed twice, CAS-Blocl^{TM} Histochemical Reagent (Thermo Fisher Scientific, Cat. 008120) was added for 10 minutes and aspirated. The specific primary antibody was added to all samples and let overnight at 4^{o}C.

Primary Antibody	Marked Structure	Dilution	Colour
Occludin Alexa Fluor® 488 conjugate	Cells' tight junctions	1:500 in CAS-Block	Green
Ki67	Mitotic chromosomes (proliferation)	1:100 in CAS-Block	-
Cleaved caspase-3	Cascade of caspases responsible for apoptosis execution	1:500 in CAS-Block	-
Anti-Vinculin	Focal adhesions	1:200 in CAS-Block	-

Table 2.1: Primary antibodies used to mark different structures, respective dilutions used and colours. Besides occludin which is already conjugated, none of the other primary antibodies are already associated with flourophores. [Occludin Antibody Alexa Fluor® 488 conjugate (OC-3F10) (Thermo Fisher Scientific, Cat. 331588); Ki67 Rabbit, (Thermo Fisher Scientific, Cat. 11357433); Cleaved caspase-3 (Asp175) Antibody (Cell Signaling Technology, Cat. 9661S); Anti-Vinculin mouse monoclonal antibody, [SPM227] (Abcam, serial D00095, Cat. ab18058)].

The next day, samples were washed three times with PBS and the secondary antibody was added for 1 hour at room temperature.

Secondary Antibody	Primary Antibody	Dilution	Colour
Goat anti-mouse 647	Vinculin	1:1000 in CAS-Block	Red
Goat anti-rabbit 488	All other antibodies	1:500 in CAS-Block	Green

Table 2.2: Secondary antibodies used to be conjugated with the primary antibodies. Occludin was already in a conjugated form with 488 fluorophore so a secondary antibody was not necessary.

Once again rinsed three times, the samples which would be stained for the F-actin distribution in the cell's cytoskeleton, Phalloidin - Alexa Fluor 568 (Fisher Scientific, Cat. 10135092) was added for 30 minutes at room temperature, at a dilution of 1:200 in PBS. After, all samples were washed, and DAPI (4',6-diamidino-2-phenylindole dihydrochloride) (Sigma-Aldrich, Cat. 32670-5MG-F) was added in a dilution of 1:100 in PBS to mark the nuclei. To finish the procedure, samples were rinsed three times with PBS and mounted on the microscopy slides with a drop of ProLong Gold Antifade Mounting Medium (Fisher Scientific, Cat. 11559306), carefully removing residual bubbles. All prepared samples were let drying protected from light for two days before imaging.

2.2.3.1 Imaging

Since sixteen samples had arrays of cavities and, in some cases, cells on the flat samples were not 2 D distributed, two dimensional images are not enough to analyse the final construct. For that reason, immunostained samples were analysed in the the live cell microscope (Nikon Eclipse Ti) in a multidimensional acquisition that can be applied by taking a sequence of images with a 1 μm of thickness (z-stack).

Images were then processed using the Nikon NIS-Elements AR Analysis 4.50.00 64-bit software. An extended depth of focus (EDF) image was generated for all acquired data.

2.2.3.2 Cell quantification

After, cell quantification for the different markers was possible using the "cell counter" option from the software ImageJ (Fiji 1.46). The total number of cells per image was obtained by counting the number of nuclei presented and the number of cells displaying the desired structure by counting the positively marked.

The last step of data processing was executed in Excel, where the graphics and respective data standard deviations were plotted and the necessary statistical analysis to check data significance was performed, using te one-way analysis of variance ANOVA test ($p<0,05$).

2.2.3.3 Metabolic Activity Assay

Cell's metabolic activity when cultured in two differently shaped PC membranes, was appraised with PrestoBlue^{TM} Cell Viability Reagent (Thermo Fisher Scientific, Cat. A13261) live assay was performed in both CALU-3 and HPAEC.

Six flat PC membranes and six curved PC membranes were treated as mentioned before and mounted in two 24-well plates, one for the CALU-3 and the other for the HPAEC. 3 wells in each well plate were used as control, 3 were used for the flat samples of polycarbonate and 3 were used for the curved PC samples. The 24-well plate for the HPAEC had to be coated for 15 minutes prior to the cell seeding.

Cells were seeded at a cell density of 70 000 cells per well and kept in culture for 11 days to take measurements in the desired time points (24 hours, 48 hours, 72 hours and 11 days), the same as in the curvature study.

A diluted solution of 10% Presto Blue with the specific culture medium of each cell type was prepared before every measurement and always kept covered to avoid light. After removing the medium and rinsing with PBS presto blue solution was added to each well and incubated for 1 hour.

After the incubation time, triplicates of 100 μL of each well were taken, as well as triplicates of the diluted solution of presto blue and culture medium (to use as blank samples and normalise the values) and transfered to a 96 MicroWell^{TM} Optical-Bottom Plate with coverglass (Thermo Fisher Scientific, Nunc^{TM} Cat. 164588) to be read on Clariostar Plate Reader (BMG LABTECH).

Since cells were kept in culture, after taking the necessary samples, cells were rinsed three times with PBS and replenished with 1 mL of fresh medium. After each time point, cells were fixed as previously described.

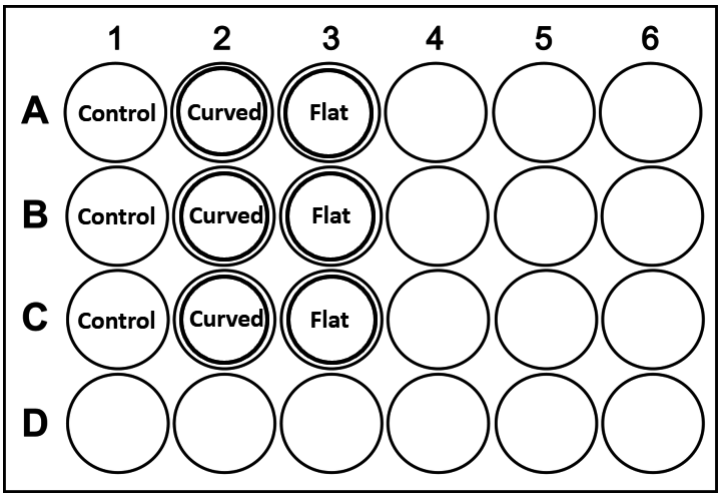

Figure 2.6: Representative template of the metabolic activity measurement. The samples with PC (3 curved and 3 flat) are fixated with black o-rings. All samples are submerged in culture medium.

2.2.3.4 Cell-Substrate Adhesion Experiment

The selected substrates for this experiment were the treated tissue culture plate of a treated 24 well plate (polystyrene) as a control, thermoformed PC membranes and non thermoformed PC membranes. Eight time points for adhesion time (15, 30, 45, 60, 90, 120, 180 and 360 minutes) were measured in triplicates. 24 curved and 24 flat membranes were punched with a size 14 of the circular cutting tool of the manual puncher, sterilised with the ethanol solutions and secured in a well plate with o-rings, as previously described for the curvature study.

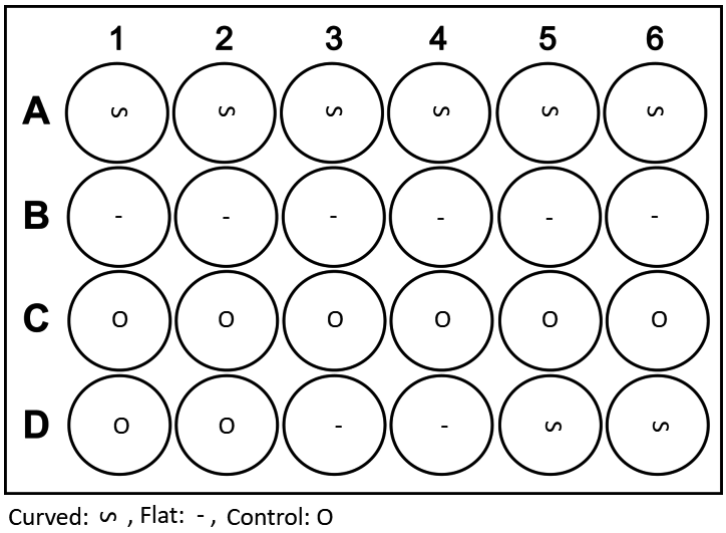

Figure 2.7: Representative template of the cell-substrate adhesion experiment display. The samples with PC (8 curved and 8 flat) are fixated with black o-rings. All samples are submerged in culture medium.

Cell density was corrected in order to have 70 000 cells per 50 μL of medium per membrane. After each time point, 500 μL of culture medium was added carefully against the well plate's wall, slowly removed and counted with the automated cell counter.

2.2.4 Air-Liquid Interface (ALI) Culture

Curved PC membranes were ion track etched for 1 hour and flat PC membranes were ion track etched for 2 hours. After rinsed in water and completely dried overnight, they were punched with size 20 of the circular cutter tool for the manual puncher.In a laminar flow hood, they were sterilised and hydrophilised following a series of ethanol and finally mounted on a CellCrown^{TM}24 insert (Scaffdex, Serial U00010, Cat. C00001N). Curved samples were mounted on the cell crown with the concave part of the cavities facing the interior of the cell crown so that cells could be cultured inside the cavities.

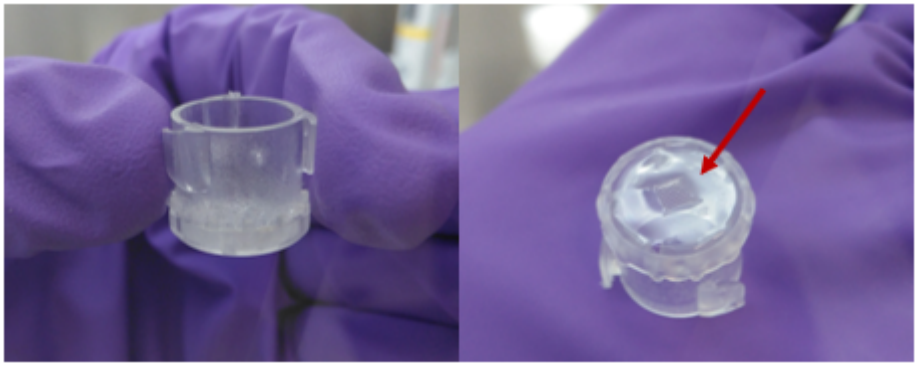

Figure 2.8: Cell crown inserts used for the air-liquid interface culture. PC curved membrane locked with the bottom part of the cavities facing the interior of the cell crown.

Firstly, 800 μL of culture medium was added to the basal compartment of the cell crown insert and 50 μL drop of culture medium was added to the apical compartment to provide coating to the membrane. CALU-3 passage 4 (P4) were trypsinised and seeded at a cell density of 70 000 cells *per well* on a cell suspension drop of 850 μL.

For this experiment it was used six curved PC samples, six flat PC samples and one treated well with cells as control. Culture medium was carefully refreshed every two days using a 0,9x40 mm needle (Fine-Ject® in the gap between the well's wall and the cell crown. The ALI culture was kept fully covered by culture medium (basal and apical surfaces) until confluence to allow proliferation and creation of a cell barrier before air exposure. The culture was carried out for four weeks, being exposed to air from week two onwards.

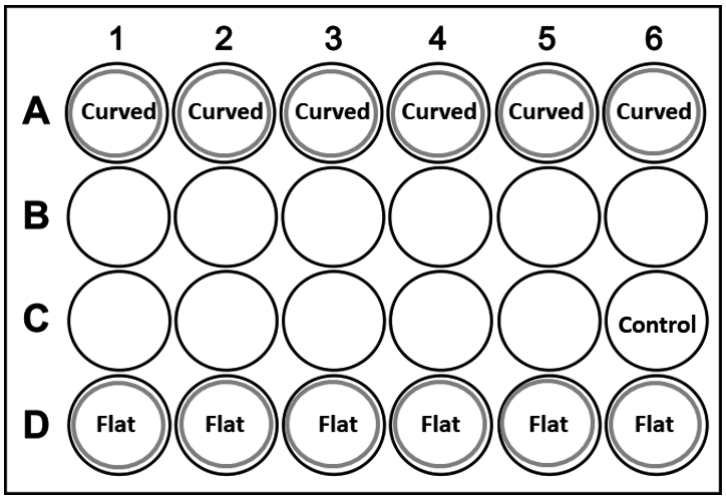

Figure 2.9: Representative template of the ALI culture experiment display. 6 porous curved PC samples and 6 porous flat PC samples are mounted in cell crown inserts in order to represent an apical and basal surface of the membrane.

2.2.4.1 Permeability Assay with Dextrans

Firstly, a dextrans calibration curve was determined for both molecular weights (3 000 Dalton and 70 000 Dalton) for the curved and flat PC etched membranes. Four different dilutions for each Dextran molecular weight were made in PBS (100%, 50%, 10% and 1%) and incubated on the apical compartment of the membranes for 1 hour. Samples taken from the basal compartment were measured in the ClarioStar plate reader and processed in Excel.

After exposing the cultured cells to air (apical compartment of the membrane on the cell crown), permeability measurements using two different molecular weighted (MW) dextrans - Dextran Texas Red® 3 000 MW, Neutral (Fisher Scientific, Cat. 41116113) and Dextran Fluorescein 70 000 MW, Anionic (Fisher Scientific, Molecular Probes^{TM}, Cat. 41116113) - were performed, starting right after the exposure (week 0) to assess the cell barrier integrity and repeating the measurement every week to assess its evolution.

For the cell barrier weekly assessment, culture medium in the basal part of the cell crown was refreshed and 500 μL of each dextran was added to the apical surface of the specific sample. All well plate was covered with aluminium foil and put to incubate for 1 hour. After, triplicates were taken for each sample, each corresponding to 100 μL of the final basal solution and put on a 96 MicroWell^{TM} Optical-Bottom Plate Plus, samples of only dextran (positive control) and samples of only culture medium (negative control) were taken and measured as well to future data analysis in Excel.

2.2.4.2 Immunofluorescence

The followed protocol was the previously described for the submerged dense PC membranes. Three primary antibody stainings were performed to mark occludin, mucin and β-Tubulin, using two dilutions for the last two in order to optimise it.

Primary Antibody	Marked Structure	Dilution	Colour
Occludin Alexa Fluor® 488 conjugate	Cells' tight junctions	1:500 in CAS-Block	Green
Monoclonal Anti-β-Tubulin IV	cells' microtubules	1:100 and 1:200 in CAS-Block	-
Anti-MUC5B	mucous cells	1 μg/mL and 4 μg/mL in CAS-Block	-

Table 2.3: Primary antibodies used to mark different structures, respective dilutions used and colours. Besides occludin which is already conjugated, none of the other primary antibodies are already associated with flourophores. [Occludin Antibody Alexa Fluor® 488 conjugate (OC-3F10) (Thermo Fisher Scientific, Cat. 331588)]; Monoclonal Anti-β-Tubulin IV antibody produced in mouse (Sigma-Aldrich, Cat. T7941); Anti-MUC5B antibody produced in rabbit (Sigma-Aldrich, HPA008246-100UL) .

Secondary antibodies are presented in **table 2.4**.

Secondary Antibody	Primary Antibody	Dilution	Colour
Goat anti-mouse 647	β-Tubulin	1:1000 in CAS-Block	Red
Goat anti-rabbit 488	Mucin	1:500 in CAS-Block	Green

Table 2.4: Secondary antibodies used to be conjugated with the primary antibodies. Occludin was already in a conjugated form with 488 fluorophore so a secondary antibody was not necessary.

One curved and one flat sample were marked with DAPI (4',6-diamidino-2-phenylindole dihydrochloride) (Sigma-Aldrich, Cat. 32670-5MG-F) on a 1:100 dilution as a nuclear stain; Occludin Antibody, Alexa Fluor® 488 conjugate (OC-3F10) (Thermo Fisher Scientific, Cat. 331588) was using on a dilution of 1:500 for the tight junctions; Phalloidin - Alexa Fluor 568 (Fisher Scientific, Cat. 10135092) on a 1:200 dilution for the F-actin distribution in the cell's cytoskeleton.

2.2.4.3 Imaging and sample's characterisation

Visualisation and multidimensional image acquisition was achieved by using a 40x oil objective lens in the live cell microscope as previously described. Image processing

was performed using the Nikon NIS-Elements AR Analysis 4.50.00 64-bit software and data analysis was supplied by ImageJ. Excel was lastly used to plot graphics, data respective standard deviations, and the necessary statistical analysis to check data significance was performed, using a one-way analysis of variance ANOVA test ($p<0,05$).

2.2.4.4 SEM - samples' preparation and imaging

To analyse the ALI's samples (cellular samples) under SEM two additional steps had to be performed. Firstly, after samples were fixed, they were dehydrated by following a sequence of EtOH and distilled water (40%, 50%, 60%, 70%, 80%, 90%, 100%) for 30 minutes each. Secondly, they were submerged for 30 minutes in hexamethyldisilazane (HMDS) (Sigma-Aldrich, Cat. 440191-100ML, serial C00729) and let dry overnight inside a fumehood. When dry, samples were mounted on SEM's stubs using a double sided carbon tape and gold sputtered for 100 seconds. An accelerating voltage of 10 kV and a working distance of 10 mm was used to image samples.

3

Results and Discussion

3.1 Fabrication of dense curved membranes

In order to achieve the desired cavity design for the cell culture platform, some combinations of parameters for the gas-assisted microthermoforming were tested and the obtained structures were quantified.

For different combinations of forming temperature and pressure, the following outputs are present in **table 3.1**.

Temperature (^{o}C)	Pressure (bar)	Mechanical Pressure (ton)	Depth ± SD (μm)
153	5	3	81,64 ± 1,54
153	8	3	106,59 ± 1,49
153	11	3	134,51 ± 5,05

Table 3.1: Variation of cavities' depth regarding the forming parameters (temperature, pressure and mechanical pressure) applied and depth's SD. 5 cavities (n_c=5) from 3 membranes' arrays (n=3) were measured for each forming parameters.

It is seen in **table 3.1** that by keeping temperature and mechanical pressure constant and varying the forming gas pressure, different depths were achieved. For a forming temperature of 153^{o}C and a mechanical pressure of 3 ton, a cavity's depth of 81,64 μm was obtained by applying 5 bar, 106,59 μm for 8 bar and 134,51 μm for 11 bar.

Since the depth value given by the laser scanning microscope (profilometer) considers the complete distance from the outer part of the top of the cavity to the external side of the flat bottom, the thickness of the tip of the cavity had to be excluded from the obtained depths. This measurements were determined using the same equipment and software.

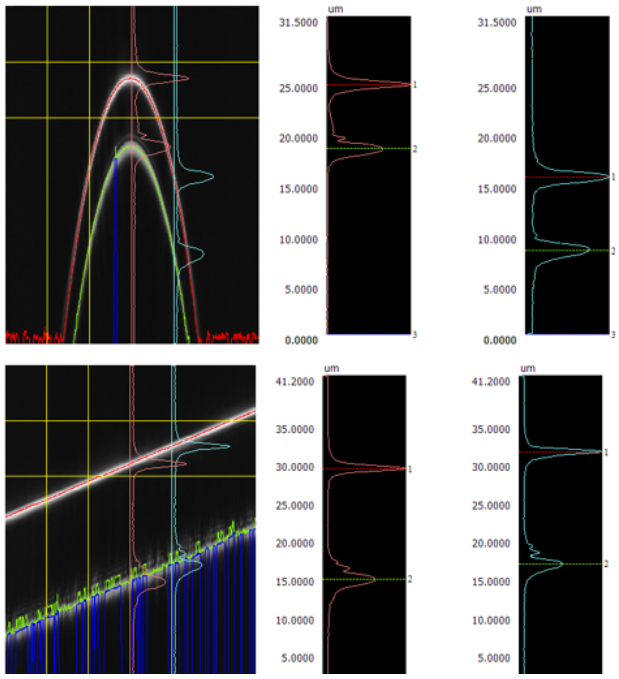

Figure 3.1: Measurement of dense membranes' cavity's thickness (top image) and flat PC film's thickness (bottom image). On the top images the interface air-thermoformed PC membrane-air are delimited by the different interaction light has with the different materials (air and polycarbonate). Two peaks (red and green) appear where the material changes, delimiting the frontier and, therefore, the cavity thickness. On the bottom image same is represented but for the flat PC membrane. n_c=5 for each thermoformed membrane's array and 5 flat areas (n_f=5) were measured on 3 different samples each (n=3).

Since this microscope uses light of a wavelength of 408 nm to detect the different interfaces, both measured thicknesses had to be multiplied by a correction factor determined by the ratio between the mechanically measured thickness (average: 24,9) and with the laser scanning microscope (average: 15).

For this determination, 5 different flat regions were marked and measured with both mechanisms. This correction factor to discover the real thickness of the PC membranes is 1,66. For the flat part of the membrane (bottom of the cavity) it was calculated a thickness of 25,15 μm which is close to the commercially stated value (25 μm).

For the top of the cavity, since this part is extremely stretched when forming, the obtained thickness was smaller, 9,80 μm. Subtracting this last thickness value to the measured depths, the available space for cell culture (real depth) is determined. Furthermore, even though maintaining the cavity's size is important, having a similar shape simultaneously is important as well.

To assess the approximate shape of the thermoformed cavity, the radius of curvature was measured. Five cavities of three different arrays were used for this purpose.

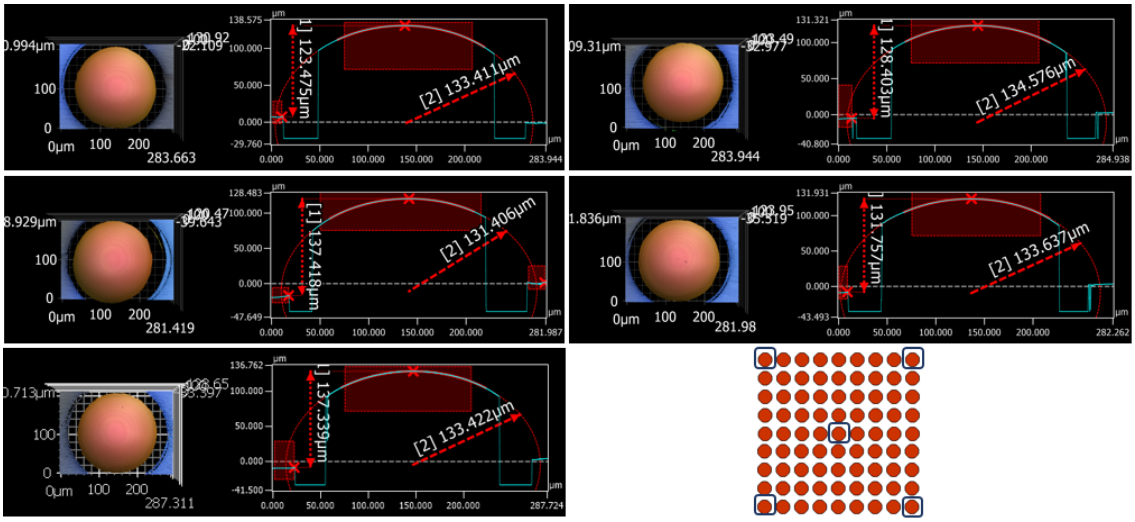

Figure 3.2: Measurements of cavities' depth and respective radius of curvature using the VK-X keyence profilometer. Five cavities (n_c=5) from the same position of each array from three different samples (n=3) were measured, as shown in the scheme on the bottom right.

Measured Depth ± SD (μm)	**Corrected Depth (μm)**	**Radius of Curvature ± SD (μm)**
81,64 ± 1,54	71,84	146,80 ± 1,12
106,59 ± 1,49	96,79	137,44 ± 0,43
134,51 ± 5,05	124,71	133,12 ± 0,48

Table 3.2: Real cavity's depth for the chosen set of microthermoforming conditions after subtracting the thickness' value from the top of the cavity. Radius of curvature values for the three different achieved depths.

From **table 3.2** it is possible to observe that for a depth of 134,507 ± 5,045 μm (with no thickness correction), the respective radius of curvature is 133,117 ± 0,481 μm, which means that the cavity resembles a half-sphere as it should. As it can be seen in **tables 3.1 and 3.2**, the best option for the project's purpose is the third set of parameters stated in **table 3.1** (153^{o}C, 11 bar and 3 ton), once the resulting depth (124, 71 μm) is the closest to the real alveolus' depth (100 μm in radius) and spherical shape [2]. This set of parameters enable the fabrication of membranes that closely resemble the human alveoli's shape and dimensions.

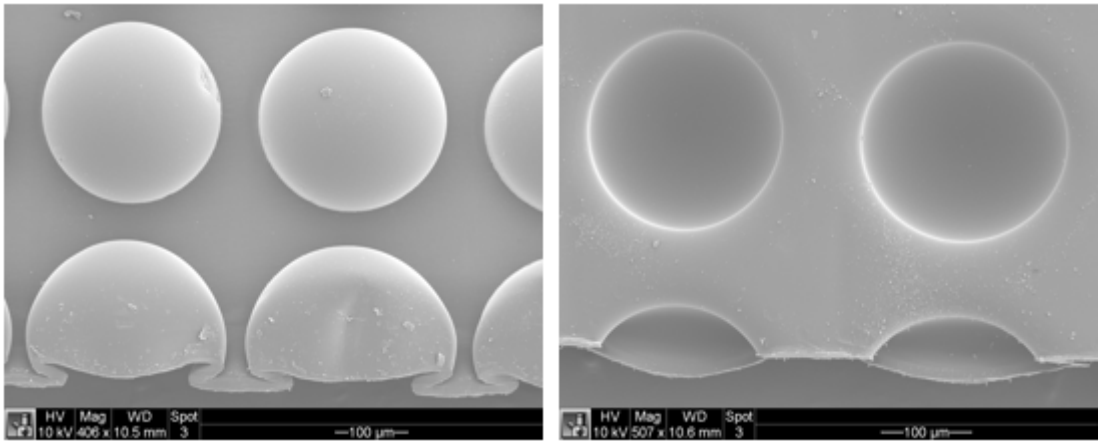

Figure 3.3: Top view (convex) and bottom view (concave) of two complete cavities on the right and left image, respectively. In both images it can also be seen two cavities cut in half which have their height structure slightly deformed due to the cutting process.

3.2 Fabrication of porous curved membranes

3.2.1 Optimisation of the ion track etching process

A more realistic model required the introduction of pores in the previously dense membrane to enable a co-culture along both sides of the membrane. For this matter, the ideal pore size created by the ion track technology had to be found and the process optimised, by varying the etching solution concentration, time, temperature and solution's motion by stirring effect.

3.2.1.1 Etched pore size on flat *vs* curved membranes

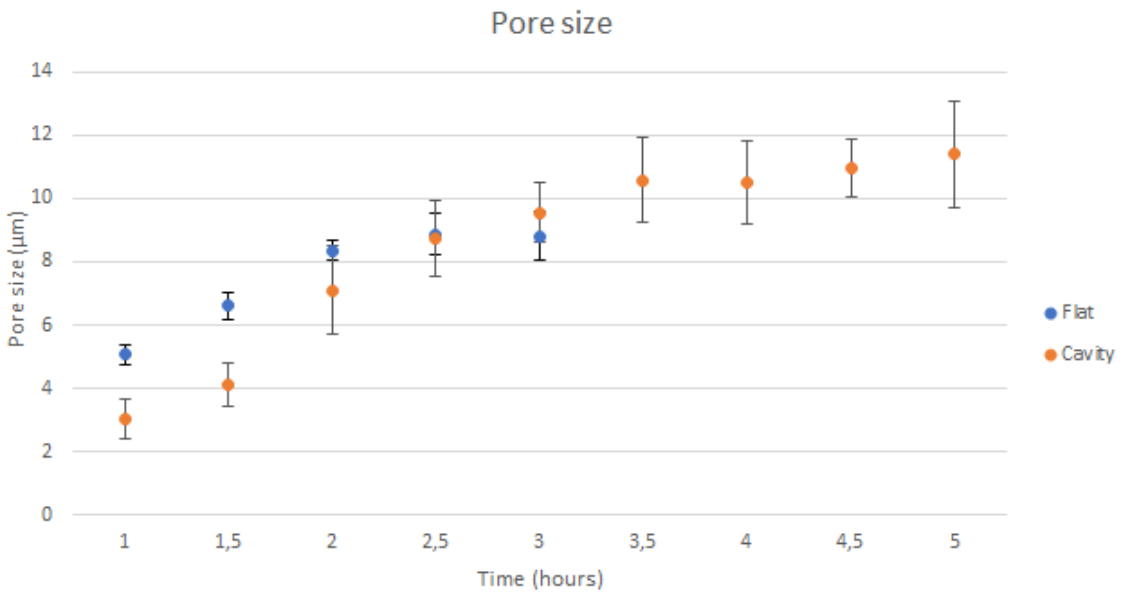

Figure 3.4: Variation of the pore's size on curved and flat membranes with the amount of hours they are etched. Triplicates for each time point for both flat and curved conditions were etched and measured. In the thermoformed samples, pores from 5 different cavities of each array were measured. In the non-thermoformed membranes pores from 5 different regions from each sample were measured. For each condition and each time point, more than 100 pores' diameters were determined.

Etching Time (hours)	Pore Size ± SD (μm)
1	3,01 ± 0,63
1,5	4,13 ± 0,70
2	7,10 ± 1,41
2,5	8,73 ± 1,19
3	9,55 ± 0,93
3,5	10,59 ± 1,32
4	10,51 ± 1,31
4,5	10,95 ± 0,91
5	11,39 ± 1,66

Table 3.3: Variation of the pore's size on the thermoformed cavities' (diameter on the surface) with the amount of hours they were being etched.

Etching Time (hours)	Pore Size ± SD (μm)
1	5,06 ± 0,32
1,5	6,61 ± 0,44
2	8,35 ± 0,30
2,5	8,87 ± 0,66
3	8,81 ± 0,77

Table 3.4: Variation of the pore's size on the non thermoformed cavities' (diameter on the surface) with the amount of hours they were being etched.

From **figure 3.4** and **tables 3.3 and 3.4**, it is possible to observe that pores get larger with etching time for both flat and curved membranes. Starting with the thermoformed PC membranes, for intervals of 1 hour, 1,5 hours, 2 hours, 2,5 hours, 3 hours, 3,5 hours, 4 hours, 4,5 hours and 5 hours, the measured pore size on the surface was around 3,01 μm, 4,13 μm, 7,10 μm, 8,73 μm, 9,55 μm, 10,59 μm, 10,51 μm, 10, 95 μm and 11,39 μm, respectively. Analysing the surface of non-thermoformed PC membrane, after 1 hour of etching the pore size was about 5,06 μm, after 1 hour and a half it was 6,61 μm and at 2 hours it increased to 8,35 μm. 2 hours and a half after the beginning of the session until 3 hour of track etching, the pore size was kept constant and it was, respectively, 8,87 μm, 9,55 μm and 8,81 μm.

Pore formation happens because when the polymer film is irradiated prior to the ion track etching session, ions create the latent track by modifying the material where the ion interacted with the polymer on a circumference around it. When submersed in etching solution, as previously explained in the introduction, polycarbonate suffers cleavage of its carbonate groups on these modified regions and pores formation starts by creating small holes on the track entries. The longer the etching, the more carbonate groups are broken and the bigger the pore gets. When the surface diameter assumes the maximum size, surfactant molecules form a thick layer and the pore formation stops.

As a remark, thermoformed arrays are composed not only by the cavities but also by flat parts in between, where cells attach, as well, so the pore size on flat parts is not only important for the 2 D ALI but also to have a better understanding of the total porosity on curved membranes.

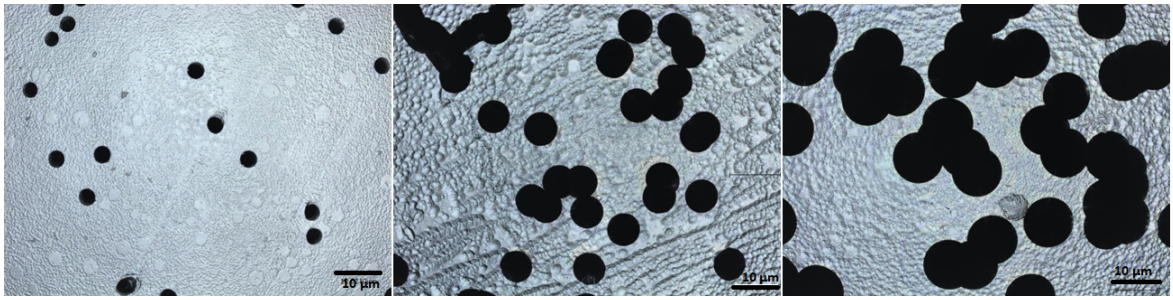

Figure 3.5: From left to right, pores' distribution and size of PC flat membranes etched for 1 hour, 2,5 hours and 3 hours, respectively.

When trying to assess if the pores were completely formed from one side to the other, a drop of isopropanol was placed on top of its surface which would be an indicator of the membrane being porous. The results pointed that for the membranes etched for less that 2 hours, the wetting with isopropanol took relatively longer compared to the rest of the samples, which indicates narrower pores. This confirms the smaller pore sizes achieved with less etching time.

Previous published applications with porous membranes for air-liquid interface used pores ranging from 0,4μm[9][21] to 10μm[11].

For cell culture, since CALU-3 and HPAEC are, in general, around 10 μm, analysing the obtained data for pore size achieved by ion track etching, the most adequate value for both flat and curved PC membranes corresponds to 1 hour of etching which produces pores of 3,01 $\pm$ 0,63 μm for the cavities and 5,06 $\pm$ 0,32 μm for the flat membranes. With these pore sizes, cells are not expected to go through the membrane due to the hole but it can be guaranteed that culture medium gets to the cell layer, providing the necessary nutrients and growth factors.

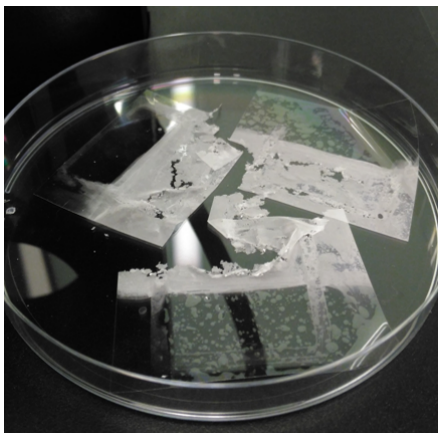

Figure 3.6: Three damaged PC flat membranes after 4 hours of etching.

Noticeable, as it is shown in **figure 3.4**, after 3 hours of etching both curved and flat PC membranes were too fragile to be handed easily in the laboratory, showing clear signs of deterioration such holes and tearing apart (as represented on **figure 3.6**). This could have happened due to the long period in contact with the alkalin etching solution at high temperature. Due to the longer the etching, the bigger the pores and thinning down the material, interconnection of pores happens after 3 hours, creating holes of 20 μm, for example.

Regarding pores overlapping, the fact that the pre-irradiation of the PC membranes is random, makes it impossible to predict where exactly the pores are going to be formed after the membrane is modified by ion track etching. After a 3 hours session, the pore size gets considerably big, resulting in larger pores that start overlapping each other, creating holes of around 20μm (as shown on figure 3.5).

3.2.2 Changes in film thickness upon track etching

As it was previously discussed in the introduction, the ion track etching solution affects, also, the bulk of the polycarbonate, representing a loss of the polymer film's thickness. The longer the polymer is being etched, the more significant is the loss of the polymer's structure, which can be easily perceived when handling the samples. They get more flexible and tend to rip apart easier.

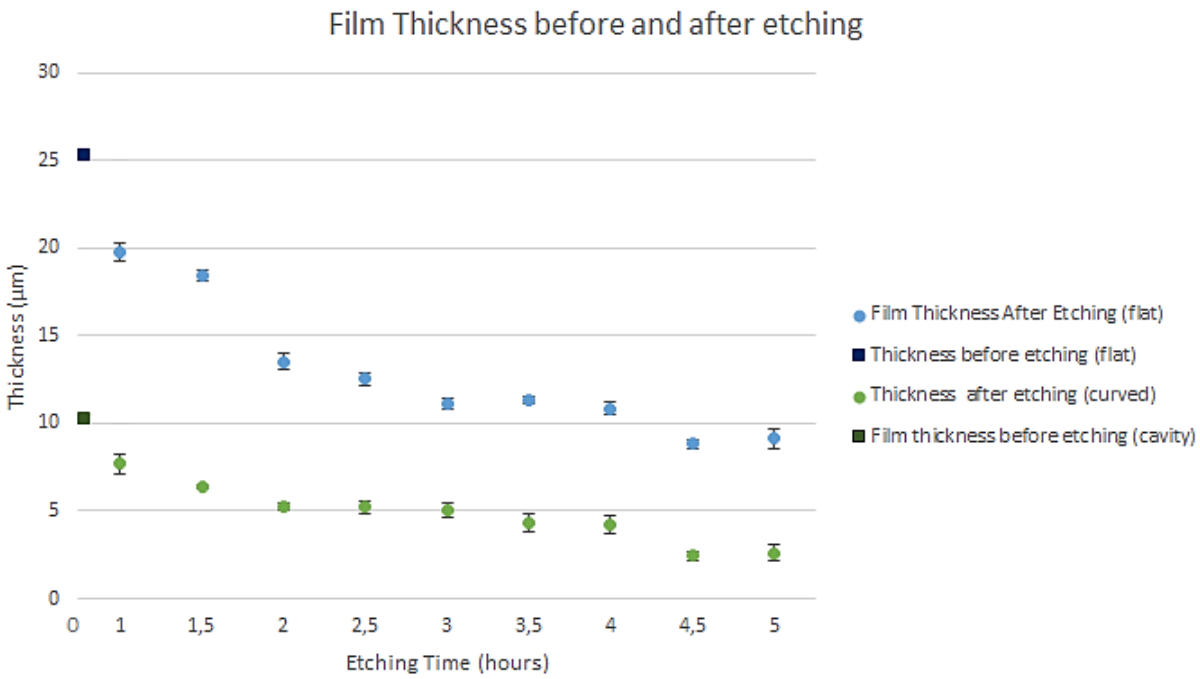

Figure 3.7: Thickness variation of thermoformed PC membranes upon ion track etching time. Thicknesses measured on top of the cavities (curved) and in between cavities (flat). Membrane's thickness before etching are represented on time=0.Triplicates for each time point for both flat and curved conditions were etched and measured with the laser scanning profilometer. Thickness from 5 different cavities of each array were measured as well as 5 flat regions (in between cavities) for each array.

It is visible that thickness for both flat and curved parts of the thermoformed PC membranes decreases with an increase in etching time. For the flat region, thickness starts as commercially stated, around 25 μm, and decreases gradually up to less than 10 μm after 5 hours of etching. For the curved part, thickness is initially 2,5 times smaller than on the non stretched flat part, starting as 10 μm and decreasing up to less than 5μm after 5 hours of etching.

This can help explaining the PC membranes' thickness loss previously referred due to the etching process.

3.3 CALU-3 cells cultured on curved surfaces

When introducing the new conformation for cell culture, it is essential to understand how cells react to it and how it does influence cell behaviour, namely regarding

proliferation, apoptosis, cell density, cell-substrate adhesion, cell-cell interaction and metabolic activity.

Firstly, to analyse how curvature influenced cell density over time, the total amount of cells (considering their nuclei) from all acquired images from all stained samples, both for flat and curved condition, for all four time points, were manually counted. Cell quantification from imaged samples had to be normalised to the flat area because the available area for cell attachment depicted in images taken with the same magnification differ from flat to curved. Cavities represent more available area than the flat surfaces due to their depth. Hereupon, knowing the diameter of a cavity 200 (μm) and applying the surface area formula for half sphere ($2\times\pi\times100^2$ = 62831,9 μm^2), measuring the image area for flat samples on ImageJ which is 89287 μm^2 and making the cell normalisation to the flat area, a correct comparison is allowed.

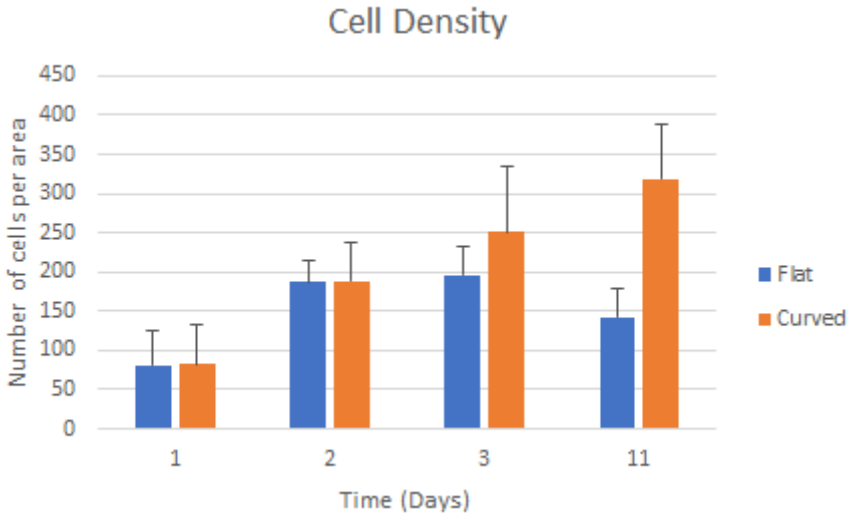

Figure 3.8: CALU-3 cell density's profile variation with time (days) when cultured on flat and curved PC membranes. Each condition of each time point is based on the total number of cells from all acquired images from stained samples. Values normalised per area. (p>0,05).

From **figure 3.8**, it's possible to observe that starting with the CALU-3 seeded on the flat PC membranes, their cell density shows a gradual increase in the first 3 days, starting with 80,71 ± 44,90 cells per area in the first 24 hours, increasing up to 186,95 ± 28,56 cells per area on the next day and showing 196,77 ± 36,37 cells after 72 hours. By day eleven, the number of cells per area decreased to 142,43 ± 37,78. For the CALU-3 seeded on the curved membranes, they represent a gradual growth in the number of cell per area from the moment they were cultured up to the last day. Starting with 82,50 ± 51,33 cells per area in the first day after cell

seeding, the number raised up 188,55 ± 48,65 cells after 48 hours, 251,01 ± 83,80 by the third day and showing a maximum of 318,23 ± 69,09 cells per area on the last day in culture.

From the results, it is possible to observe that in general there are more cells in the cavities when compared the same area on the flat surface and that by day eleven the difference is more striking. However, the statistical analysis ANOVA confirms that the difference observed for curved and flat results are not statistically significant which might suggest that these values simply follow a tendency to eventually differ. One of the reasons why the alveoli are "pocket" shaped and the majority of the human organs have curved anatomies is to maximise their superficial area in order to optimise the necessary exchanges. For this reason and regarding cell density, it makes sense that after eleven days in culture and after reaching confluence, once in the thermoformed membranes there is more available space considering the cavity empty space, there is a bigger cells count. These observations can be supported and better understood by the 3 D reconstructions of the CALU-3 inside the cavities, as shown on figure 3.9, where it can be easily observed the formation of 3 D colonies (clumps) growing vertically inside the cavity.

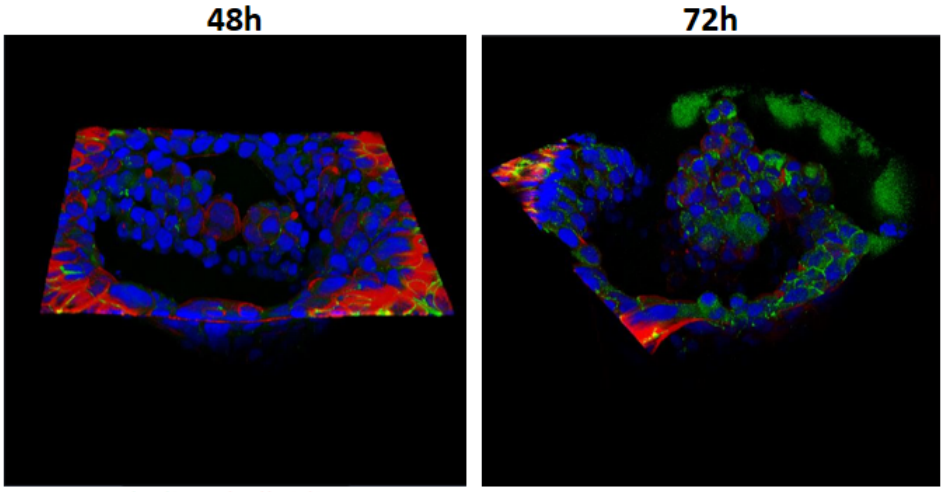

Figure 3.9: 3 D-reconstruction of the cavities with CALU-3 cultured inside for two time points: 48 hours and 72 hours after cell seeding. Immunostaining: DAPI for the nuclei, occludin for the tight junctions and phalloidin for the cell's cytoskeleton F-actin.

From the analysis of how CALU-3 grow when cultured on a curved substrate, it is distinguishable that on the flat membranes they form a typical flat colonies while, on the cavities, firstly they form clumps and then they spread to cover the rest of

the substrate. This results might be supported by **figure 3.10** where images of the cells on curved and flat membranes are display for all four time points.

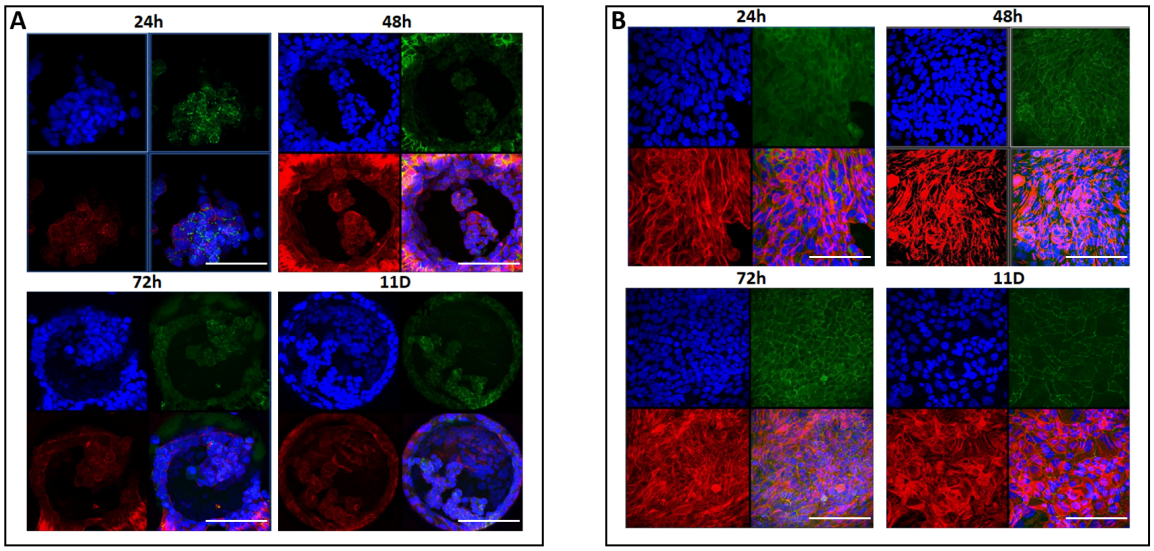

Figure 3.10: Left image (**A**): 3 D top view of the cavities with the CALU-3 cultured inside. It is possible to see the different cell densities and cell arrangements with time (days). Right image (**B**): CALU-3 cultured on PC flat membranes for eleven days. Immunostaining: DAPI for the nuclei, occludin for the tight junctions and phalloidin for the cell's cytoskeleton F-actin. Scale bar: 100 μm.

Regarding the thickness of the cell layer CALU-3 form while proliferating and spreading over the cavities' walls and flat membrane, it can be observed that its shape and height change depending on how long the cells are in culture. **Figures 3.11** and **3.12** depict how the cell layer thickness varies with time after cultured based on cross section images taken with a confocal microscope. In figure 3.11, in the first 48 hours after cells were seeded the cell layer is thick, cells have a round shape and they associate with each other forming clumps. After 72 hours, it is still possible to see the clumps on the top of the cross section image but at the bottom cells are starting to get flattened and are not displayed as 3 D colonies. In both time points, cells do not cover the totality of the cavity wall. By day eleven, it is noticeable the thickness' difference when compared to the previous discussed. The cell layer is notoriously thinner, cells are longer instead of round and they are covering completely the cavity wall.

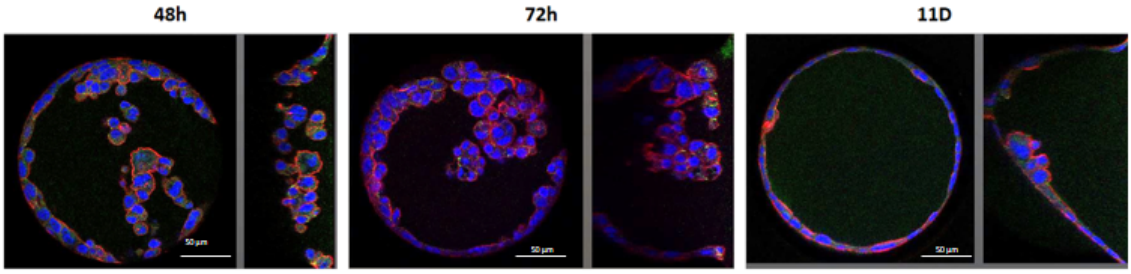

Figure 3.11: Cell layer thickness' variation with time in culture for curved membranes. Immunostaining: DAPI for the nuclei and phalloidin for the cell's cytoskeleton F-actin. Scale bar: 50 μm.

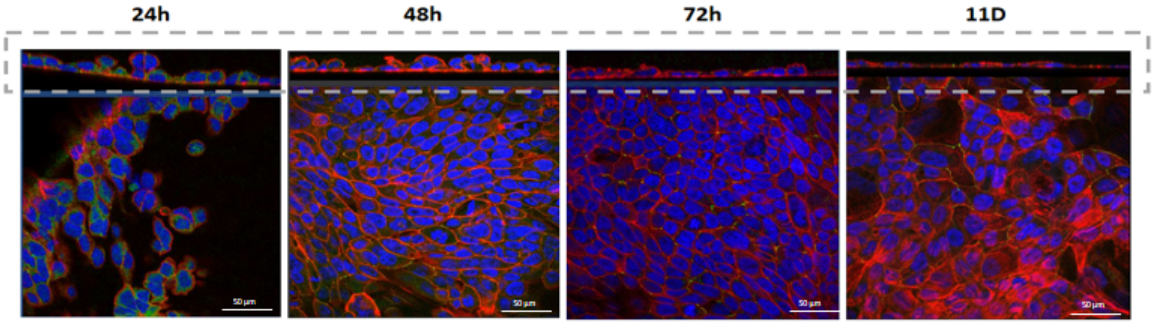

Figure 3.12: Cell layer thickness' variation with time in culture for flat membranes. Immunostainings:DAPI for the nuclei and phalloidin for the cell's cytoskeleton F-actin. Scale bar: 50 μm.

It is understandable that a bigger amount of cells could grow and spread on the curved membranes, creating firstly 3 D colonies and growing with the height of the pocket. These cells interact differently than on a flat 2 D membrane because the curvature influences the angle they assume when attaching to the surface and, therefore, affecting in which and in how many points they interact with contiguous cells. The fact that CALU-3 completely line the cavities' wall, that monolayer gets thinner with time and that there are more cells per area might have a positive impact on the cell barrier function for a future air liquid interface application of the same structure but porous.

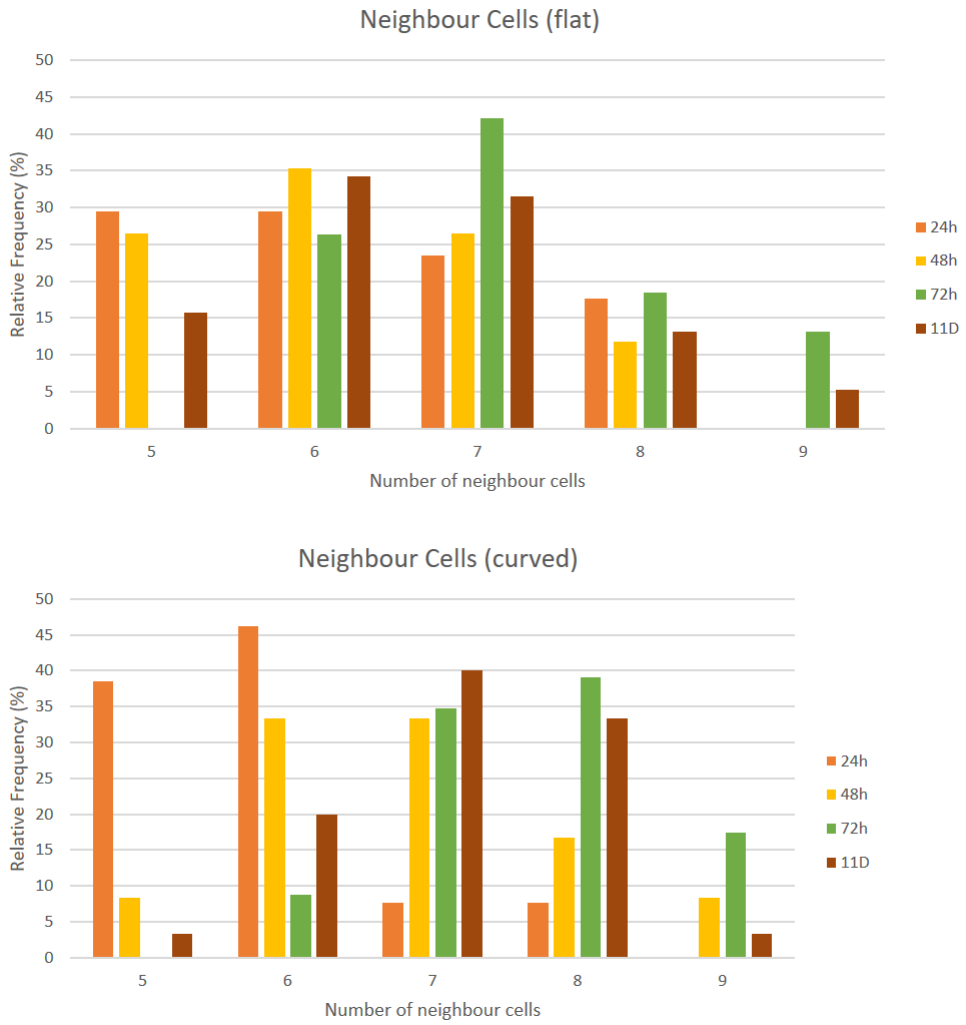

Figure 3.13: Number of neighbour cells in relative frequency on flat membranes (top) and number of neighbour cells in relative frequency inside cavities (bottom). Values normalised per area.

One of the main characteristics of the CALU-3 is the capacity of creating good tight junctions, which affect, as well, the cell barrier function. Already shown that there are more cells per area, it is assumed that more cells are in contact with each other, forming important tight junctions.

Figure 3.13, plots results for the number of neighbour cells on flat and curved membranes. It is possible to see that, in general, more cells surround one single cell inside cavities when compared to flat 2 D membranes. Starting with the quantification on flat membranes, the maximum number of cells surrounding a single cell is 9 and it was visible for samples cultured for 72 hours and 11 days in culture. For this substrate, the most repeated result is that 6 or 7 cells are in direct contact with one for all time points.

For the cavities, the maximum number of cells neighbouring one single cell was 9, as well, but this was visible for the last three time points (48h, 72h and 11 days) meaning that cells are surrounded by more other cells sooner than on flat substrates. The normal number of cells in encompassing one cell is between 7 and 8.

This proves that, generally, inside the cavities, cells are in contact with more cells than on flat membranes, as expected by the induced angles the curvature forces cells to adapt.

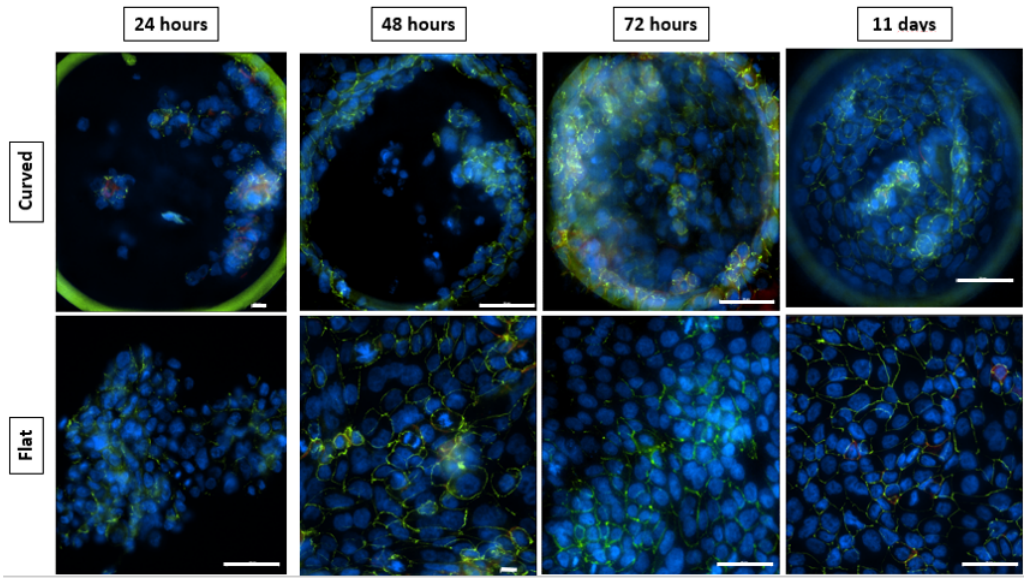

Figure 3.14: Occludin immunostaining to show the tight junctions formed by CALU-3 with their contiguous cells. Immunostainings:DAPI for the nuclei, occludin. Scale bar: curved 24h and flat 48h - 10μm; other images: 50 μm.

3.4 Impact of curvature on cell's metabolic activity

Besides quantifying the metabolic activity on the defined time points for the curvature's study, daily measurement were performed for the CALU-3, in the same conditions, with an additional control with cells only cultured on the treated well plate surface (polystyrene).

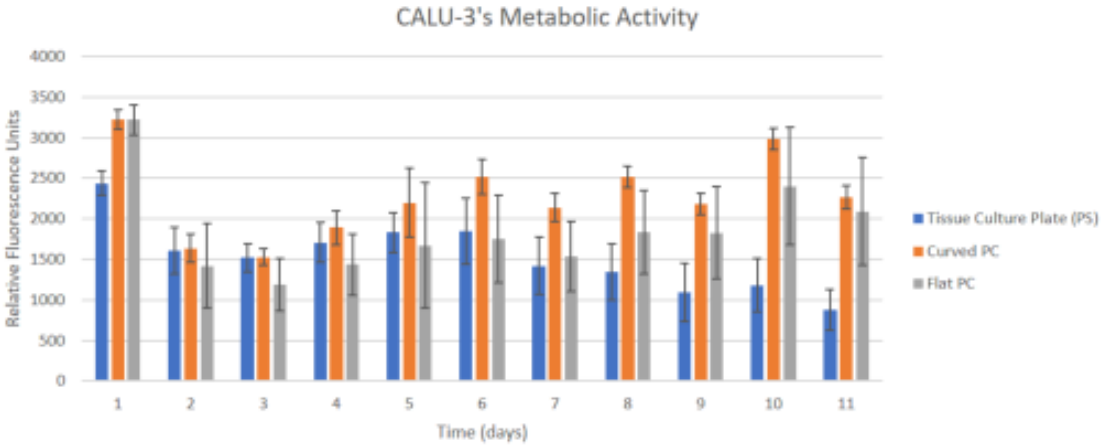

Figure 3.15: CALU-3's metabolic activity (presto blue digestion) on the treated tissue culture well plate (polystyrene) and on curved and flat PC membranes measured for 11 days. (p>0,05).

The immediate first day after cell seeding is mainly for cell attachment to the surface, where the cell's cytoskeleton reappears, enzymatic activity increases and the synthesis of DNA and structural proteins as well [62]. On **figure 3.15**, regarding day 1, it's visible a higher metabolic activity for the cells cultured on PC membranes (curved and flat) when compared to the control (polystyrene). From day 2 to day 6, control has relatively higher metabolic activities when compared to the flat PC membranes, inverting this pattern from day 7 to day 11. Metabolic activity of the CALU-3 in thermoformed membranes is always bigger than the other two conditions. Comparing curved PC membranes specifically with flat, metabolic activity is maintained higher, as already stated, but the standard deviation of flat values have to be taken into consideration, which might be translated in not statistically significant differences.

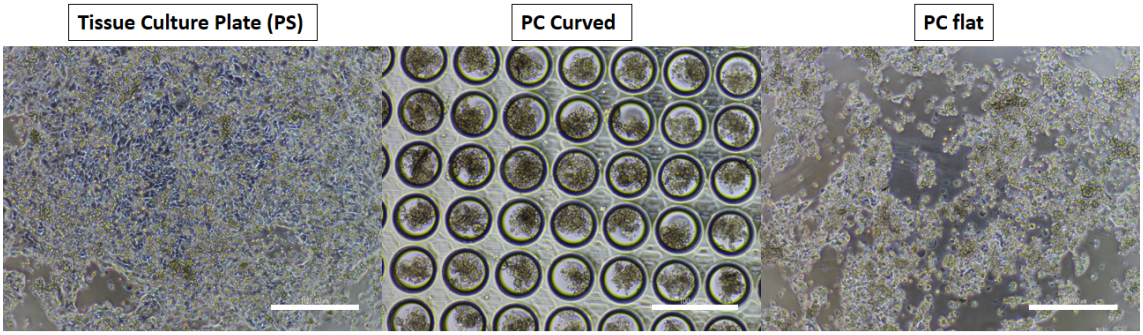

Figure 3.16: Day 1 of CALU-3 cultured as control (on the polystyrene well), PC curved membrane and PC flat membrane, from left to right, respectively. It's noticeable how some cells are not attached, stacking on top of each other. Images taken with an inverted microscope (Nikon Eclipse TS100). Scale bar: 300 μm.

However, the represented higher metabolic activity in the thermoformed membranes might be explained by the fact that even though the material is the same, a different conformation introduced by the curvature influences cells to waste more energy to adapt, attach and interact with other cells while assuming different spacial angles. This can show a sensed impact provided by geometry on their adaptation, as well as a possible positive influence for these lung epithelial cells for being in a conformation closer to reality. Attention has to be paid to the statistical analysis from ANOVA which confirms that the difference observed for curved, flat and control are not statistically significant which might suggest, once again, that these values simply follow a tendency to eventually differ.

3.5 Impact of curvature on cell proliferation

To assess how curvature influenced cell proliferation rate over time, the number of positively marked cells and the total amount of cells (considering their nuclei) from 5 acquired images for each condition (flat and curved, for all four time points), were manually counted. Area normalisation was performed as previously described.

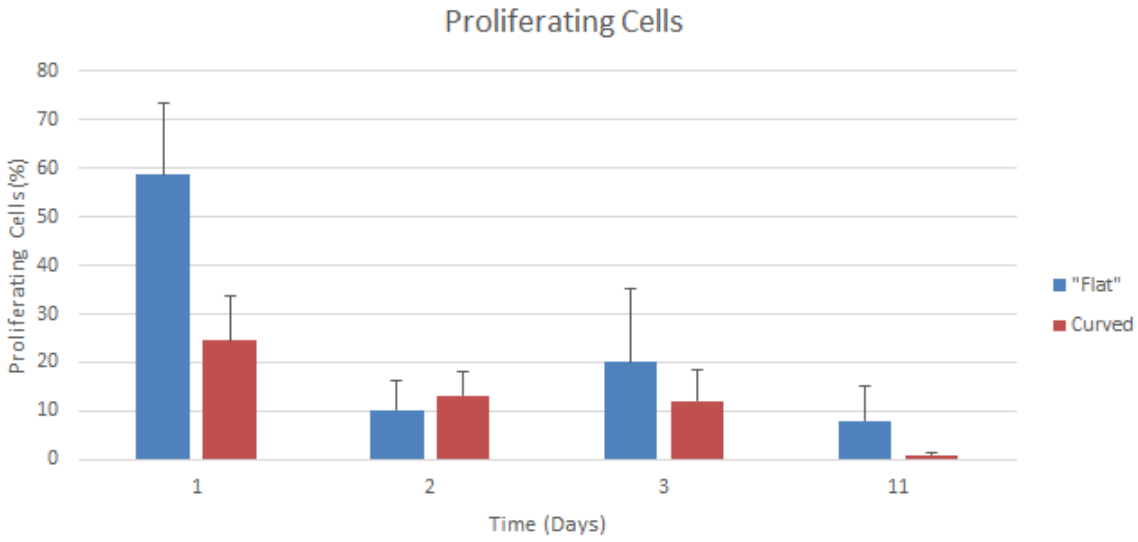

Figure 3.17: CALU-3 proliferation profile variation with time (days) when cultured on flat and curved PC membranes. Each condition of each time point is based on 5 acquired images for the Ki67 staining. Values normalised per area. ($p>0,05$).

Regarding cell proliferation on the curved membranes, one day after seeding 24,51 ± 11,31% of the cells were proliferating, decreasing to 13,10 ± 5,92% on the next day and, on the third day, 12,16 ± 4,51% of cells were proliferating. By day eleven,

only 0,98 ± 0,62% of the cells were proliferating. On the flat membranes, 58,63 ± 14,40% of the cells were proliferating on the first day, decreasing to 10,27 ± 5,88% after two days in culture, increasing to 20 ± 15,06% on the third day and finally decreasing to 8,04 ± 6,96% by day eleven.

These are expected results once cells tend to proliferate at a bigger rate in the first day after seeding, slowly decreasing their proliferation as confluence is achieved and, after reaching it, the proliferation percentage assumes low values. Besides day 1, where it is possible to observe that cells tend to proliferate more on the 2 D PC substrate, from day 2 inwards the difference between flat and curved is not so noticeable. Further more, statistical analysis with one-way ANOVA states that the difference observed for curved and flat is not statistically significant which might suggest that these values simply follow a tendency for their proliferative activity. This permits to conclude that lung epithelial cells do not seem to have their proliferation rates inhibited due to the new conformation, which may have an affect on cell barrier regeneration when disrupted.

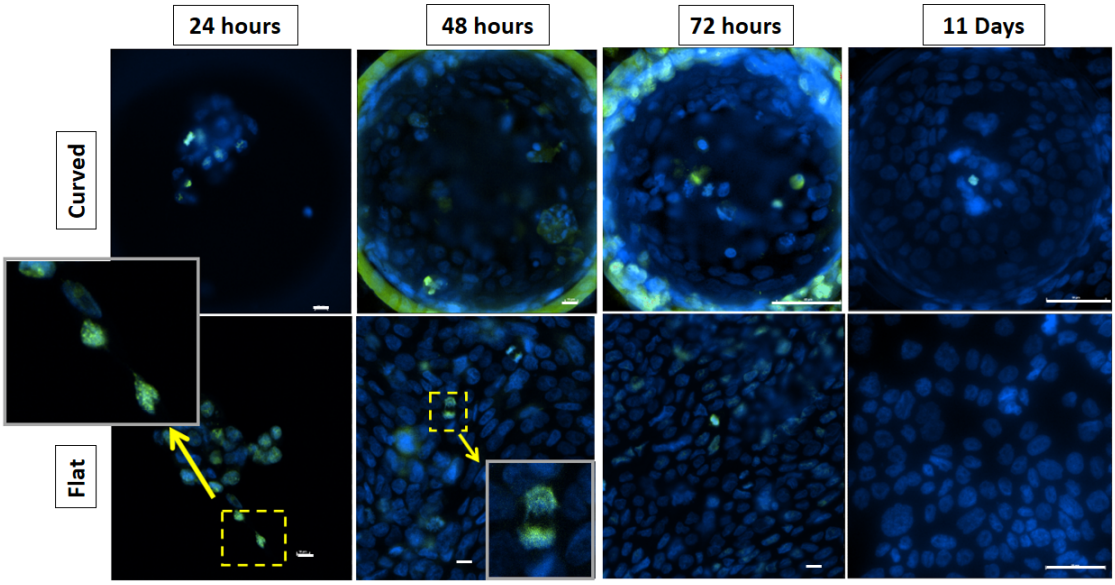

Figure 3.18: Images from proliferating cells on the curved and flat membranes. In the two close-ups it is possible to see (from left to right) cells on the telophase and cytokinesis, respectively. Immunostainings:DAPI for the nuclei, ki-67 for mitotic chromosomes (proliferation). Scale bar: curved 24h, 48h; flat 24h, 48h, 72h - 10μm; other images - 50μm.

An additional result concerning cell proliferation inside the cavities may be seen in **figure 3.19**. Images from 48 hours and 72 hours after cell seeding show a bigger number of positive cells for proliferation on the interface from flat to curvature than

on the flat or inside the cavity itself. This might be proof that topography and conformation affect cells' behaviour, inducing or inhibiting their basic activities. In this specific case, promoting cell proliferation.

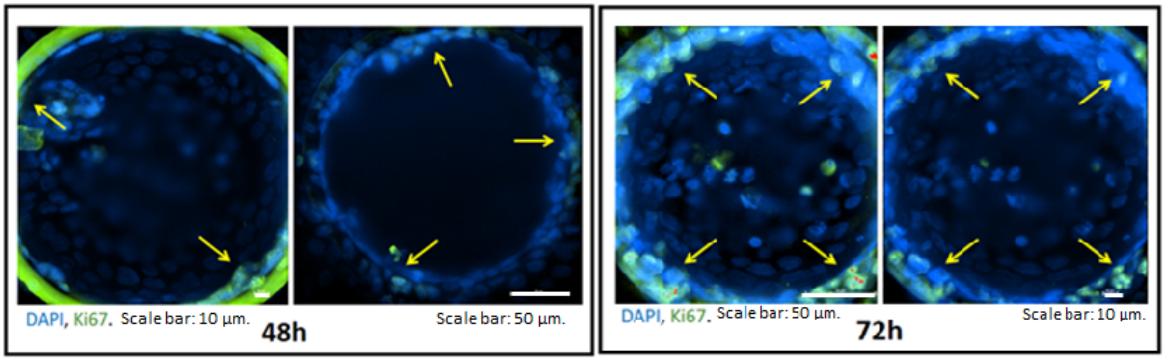

Figure 3.19: Emphasis on the higher number of positive cells for proliferation on border interface from the flat domain to the curved part of a cavity. Samples kept for 48h and 72h in culture. Immunostainings:DAPI for nuclei, ki-67 for mitotic chromosomes (proliferation), Scale bar stated for each image.

This interesting result makes it questionable how CALU-3 react to different substrate shapes, from 2 D (what has been used on human alveoli *in vitro* models) to 3 D cavities, and why is the proliferation rate higher when passing from a flat profile to a curve one. To take into account that this pattern on the border is only observable after 48 hours after cell seeding probably because there are not enough cells going from the flat part of the thermoformed membrane into the curvature before.

3.6 Impact of curvature on cell apoptosis

Apoptotic cell counting and area normalisation were performed as described for proliferation, considering the positively marked cells for caspase-3.

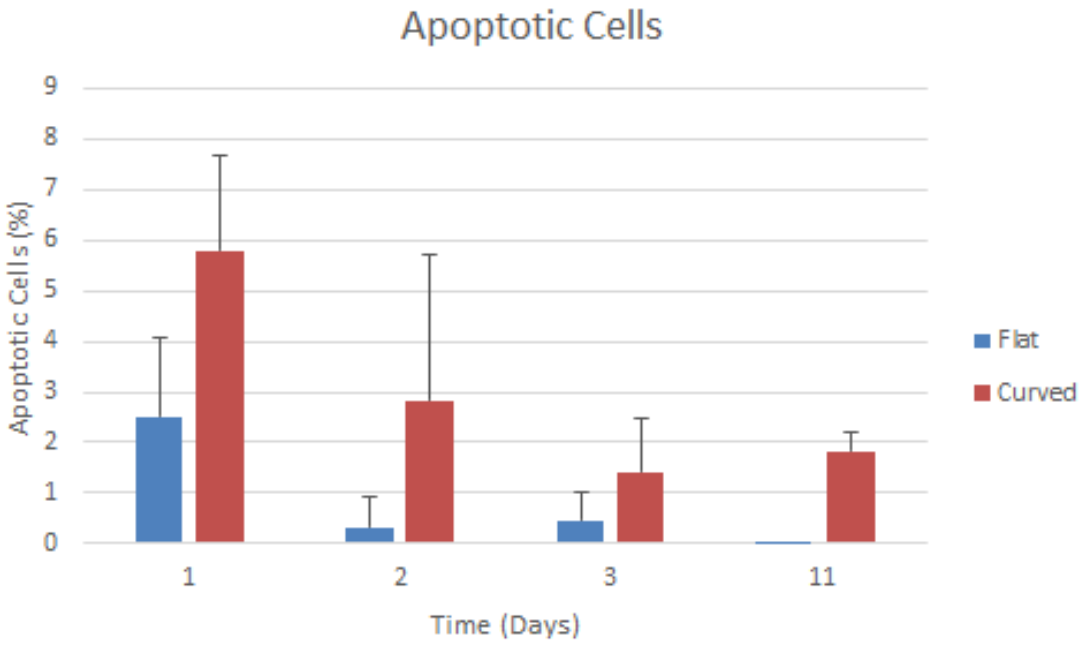

Figure 3.20: Apoptotic cells rate for curved and flat dense PC membranes cultured for eleven days. Each condition of each time point is based on 5 acquired images for caspase-3 staining. Values normalised per area. ($p>0,05$).

The percentage of apoptotic cells on the curved membranes 24 hours after seeding is 5,79 ± 2,20%, followed by 2,84 ± 3,32% after two days in culture, falling to around 1,42 ± 1,07% on day three. By day eleven, 1,83 ± 0,42% of the cells inside the cavities are suffering from programmed death. Regarding apoptosis of the CALU-3 on the flat membranes, around 2,52 ± 1,56% of the cells are apoptotic in the first day after seeding, falling to to less than 1% in the next two days (time point of 48 hours: 0,31 ± 0,63% and 72 hours: 0,46 ± 0,55%) and the percentage of apoptotic cells is null by day eleven. Applying the statistical analysis ANOVA, the visible difference for curved and flat is not statistically significant which might suggest that these values simply follow a tendency regarding apoptosis rates.

As a first approach, it is important to notice that these percentages of apoptosis are very small (smaller than 6%). In general, and looking in detail, apoptosis levels are higher inside the cavities when compared to the flat membranes. However, this doesn't necessarily translates as adverse for the cell culture. The fact that cells suffer apoptosis is mainly to maintain healthy cells in culture without wasting unnecessary energy with damaged ones or non viable ones.

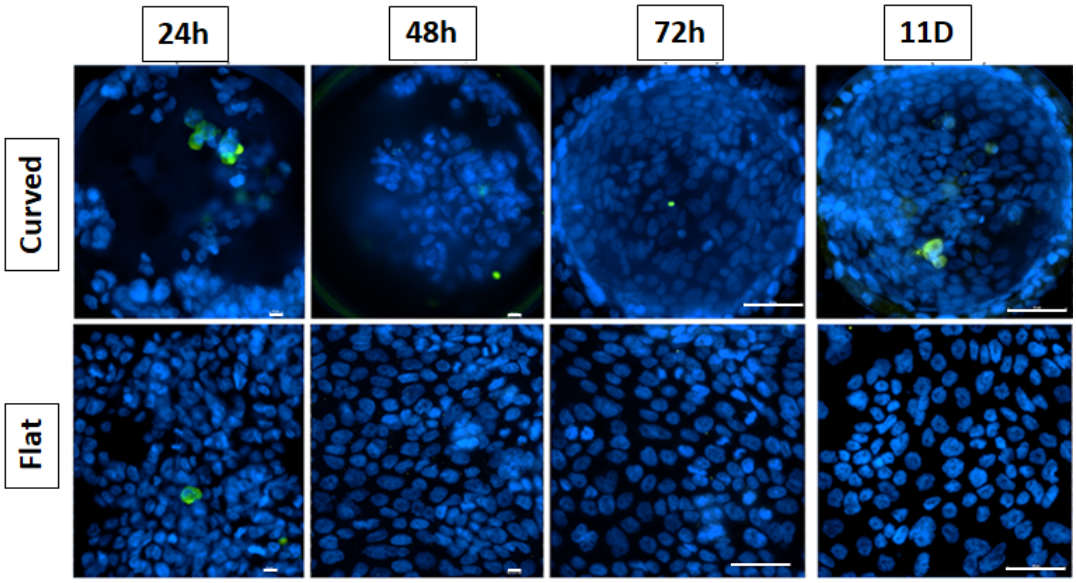

Figure 3.21: Images from cells marked for apoptotic cells. Immunostaining DAPI for nuclei, caspase-3 marking apoptotic cells in both curved and flat PC membranes for all time points. Scale bar: 24h and 48 hours - 10 μm; 74h and 11 days - 50 μm.

Furthermore, studies already showed that curvature forces cells to be confined to narrow regions, becoming more rounded, increasing their cytoskeleton's flexibility [63] that may induce intracellular structural rearrangements which might be lethal. This increases apoptotic index [64] when compared to cells' behaviour observed on flat membranes. Not only cell's spreading is affected but also ECM adapts curvature [64], influencing cell-ECM contact area and, therefore, the cellular survival rate. On **figure 3.21** it is possible to see that positively marked cells for apoptosis are mainly on the centre of the image and, therefore, belong to the smaller region of the cavity - the tip. These results might have an impact on cells renewal, which is necessary for the good function of the cell barrier.

3.7 Impact of curvature on cell adhesion

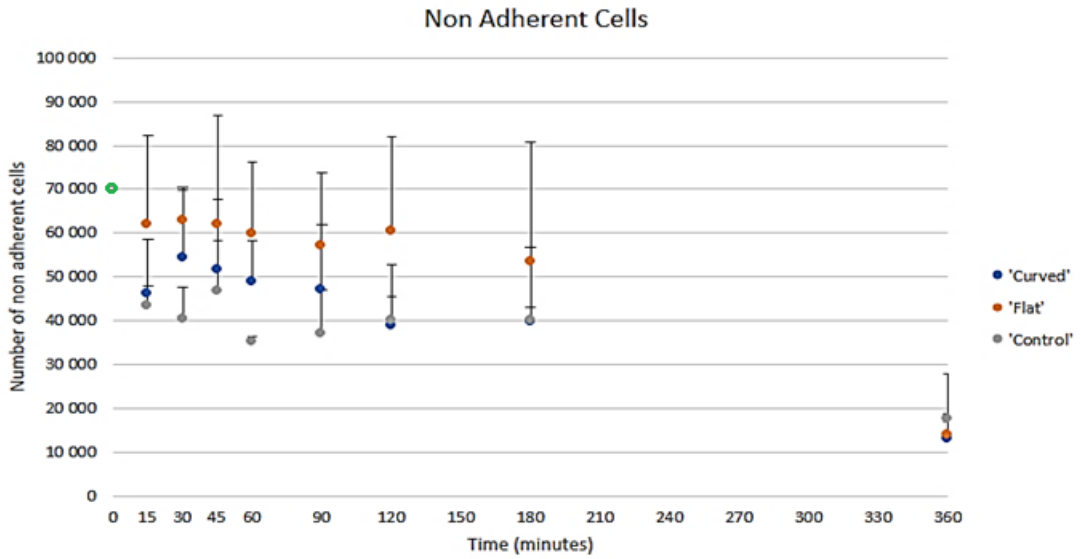

Figure 3.22: Non cellular adhesion profile with time for CALU-3 cultured on a control (treated tissue culture well plate) and curved and flat PC membrane. Triplicates for each condition for every time point were counted. Green point for time=0 represents the cell seeding density for all three conditions (70 000 cells per well).

As it is shown in the **figure 3.22**, it was tested how differently CALU-3 would adhere when cultured in three different substrates: a thermoformed PC membrane, a non thermoformed PC membrane and polystyrene of the normal treated cell culture well plate (control). By the direct analysis of **figure 3.22**, 15 minutes after cell seeding there was a noticeable decrease in the number of cells counted for all three substrates. On the control, the number of cells that did not adhere was 43 333 cells per millimetre, representing the smaller amount of all three conditions. On the curved membranes, a slightly higher number of 46 117 non adherent cells was counted. Relatively to the flat PC membrane, the number of non adherent cells was larger, collecting 61 783 cells from the well, a value too close to the initial cell seeding density. From the first time point until 3 hours after seeding, the number of cells counted decreases in a very slow rate, always maintaining the described pattern of non adherent cells for the three conditions.

However, it is necessary to keep in mind that both curved and flat PC membrane are from the same material, only differing where the 81 cavities are, which is a small percentage when compared to the whole well plate. For this reason it wouldn't be

expected to have such a difference in the cell adherence profile for both curve and flat polycarbonate membranes. One possible explanation for the supposed better adherence of the cells on the curved membrane rather than on the flat ones, represented in the graphic, might be due to the fact that when cells are seeded directly on top of the cavities' array, a big fraction of them fall inside the cavities by gravity's action and get trapped. When medium is added against to the well's wall to make the count of non adherent cells, most remain inside the cavities' even though they might not be attached to the substrate yet. Getting trapped, in this situation, is not necessarily a negative aspect. Cells stay inside the cavity with culture medium and settle by gravity, adhering with the necessary time required which might be similar to the time taken by cells to adhere on the flat membranes represented in the graphic. From this, cells adhere and proliferate covering the surface, as seen in all experiments using thermoformed cavities.

From the graphic analysis it can be understood that an incubation time of, at least, 3 hours after cell culturing is the most efficient way to preserve the maximum number of cells in culture for all three tested substrates.

3.8 Air-Liquid Interface of CALU-3 on curved surfaces

The ALI culture is a set up that can be used to approximate *in vitro* alveolar models to reality by exposing epithelial lung cells to air, (which mimics the interior of the human alveoli), while simultaneously in contact with culture medium, (mimicking the human blood).

It was chosen to use porous membranes fabricated by ion track technology instead of the already commercially available ones. For the curved membranes, pores were only produced after forming the cavities because it is necessary that the PC film is dense when gas-assisted thermoforming, otherwise gas would pass through the pores of the film and no cavity would be formed.

When exposing the CALU-3 to air, they are expected to develop cilia and to produce more mucus than when submerged in culture medium. Since it was the first ALI being completely finished and studied by specific immunostainings, optimisation for mucin and β-tubulin concentrations was performed.

3.8.1 Impact of curvature on the barrier function

Two different dextran sizes were selected (3 000 kDa and 70 000 kDa) in order to define the cell barrier's permeability limits by and understanding how tight cells were when forming the confluent cell layer.

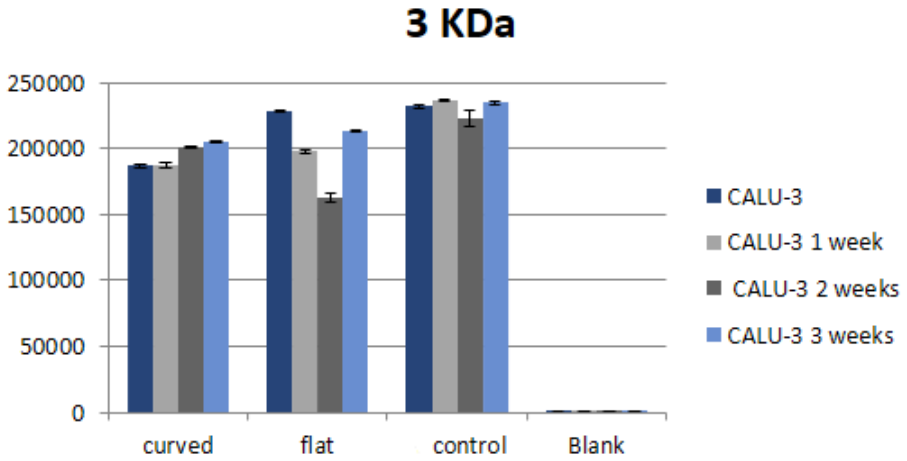

Figure 3.23: Weekly variation of the permeability profile of the formed cell barrier for the smaller dextran size (3 000 Dalton). Both positive control (signal of only dextrans) and blank (signal from culture medium) are plotted as well. Blank values were used to correct the measured signals in the curved and flat samples.

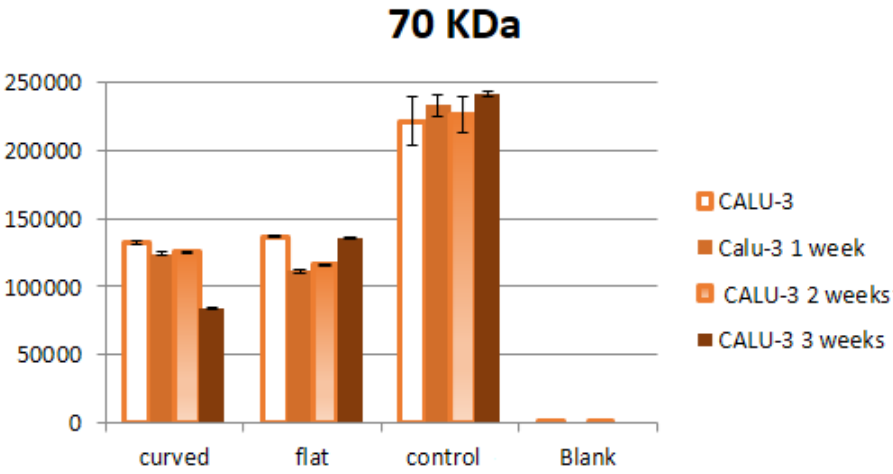

Figure 3.24: Weekly variation of the permeability profile of the formed cell barrier for the bigger dextran size (70 000 Dalton). Both positive control (signal of only dextrans) and blank (signal from culture medium) are plotted. Blank values were used to correct the measured signals in the curved and flat samples.

Even though it was expected a decreasing signal over time due to the decrease on the

cell barrier's permeability due to stronger tight junctions, that was not observed for any case (curved or flat, bigger or smaller molecular weight). It's visible that for all conditions, at least one of the weeks' measurements exhibits a higher readout, which was not supposed to happen if the cell barrier was, in fact, getting more cohesive with time in culture, making these results inconclusive. However, a positive aspect on both molecular weights' graphical representation is shown by the difference in the fluorescence signal between 3 000 Da and 70 000 Da. It is expected a lower permeability to big sized molecules rather than to small ones.

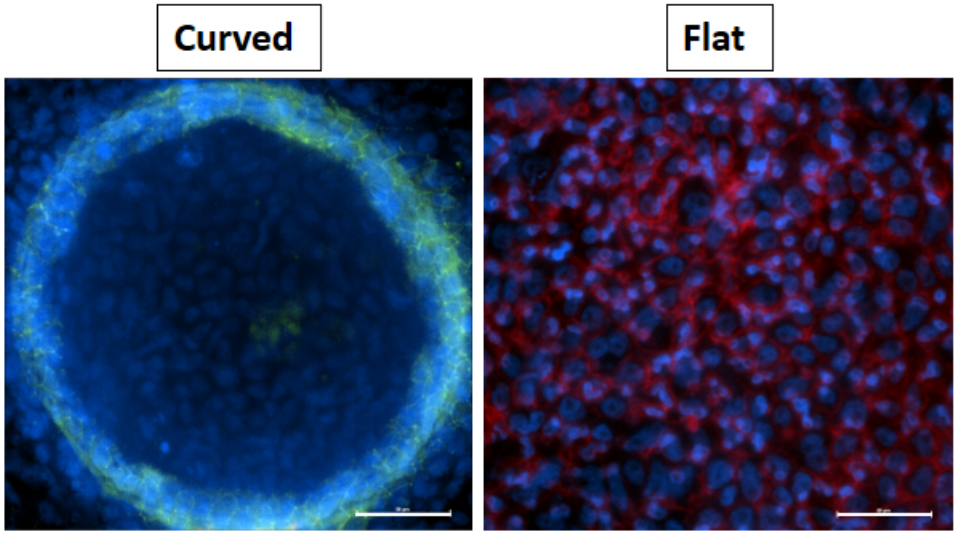

Figure 3.25: CALU-3 forming a uniform cell layer covering totally the flat membrane and the cavity's wall (left image, immunostaining:DAPI for the nuclei, occludin for the tight junctions; right image, immunostaining: DAPI for the nuclei, phalloidin for the cell's cytoskeleton F-actin) Scale bar: 50 μm.

As a first approach to this results it would be expected something wrong with the cell barrier's integrity and these fluorescence peaks would happen due to a non confluent and tight cell barrier. However, this is not the case since it can be seen by the immunostained samples on **figure 3.25** that both flat and curved membranes are fully covered by lung epithelial cells. Furthermore, on **figure 3.26**, tight junctions are present in both samples, proving that besides confluent, cells are tightly connected.

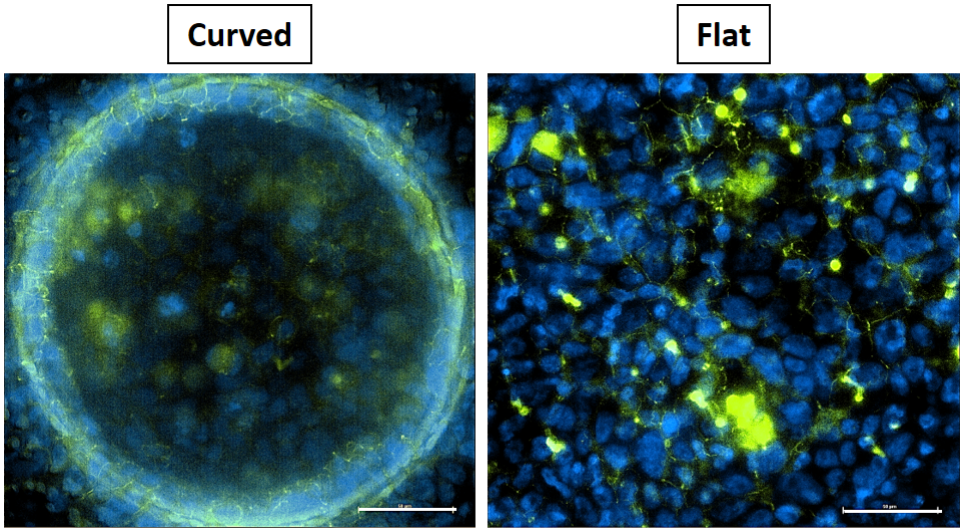

Figure 3.26: Tight junctions formed by CALU-3 as a uniform cell layer covers the surface of the cavity (left) and the flat membrane (right). Immunostaining:DAPI for the nuclei, occludin for the tight junctions; Scale bar: 50 μm.

Aside from the fact that this was the first attempt to assess cell barrier's permeability when exposed to air and that the ALI setup is far from being optimised, these unexpected results might be explained by the visible holes on the samples and by a possible leakage on the walls of the cell crown inserts that are thought not to seal completely. It is important to remind, as shown in the beginning of this study, that PC membranes get fragile when etched when compared to already commercially porous membranes.

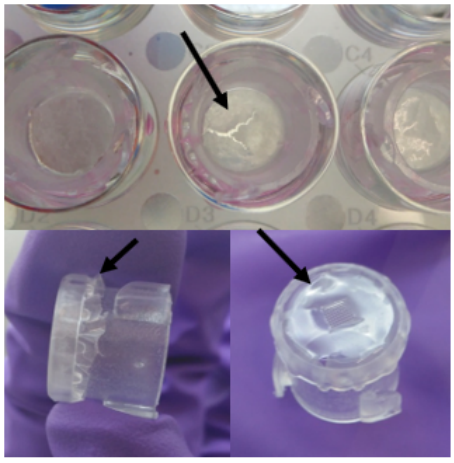

Figure 3.27: Cell crown inserts with PC thermoformed and non thermoformed membranes. It is possible to see holes on the flat membrane and the tension the insert applies on such a small area of the circular membrane.

Besides the brittleness of the etched membranes previously discussed, the presence of pores also influenced imaging in the sense that in some circular spots (pores) the signal was very intense, making it more difficult to acquire a good image for the desired structure to be analysed.

It has to be considered that this ALI culture trial serves as a preliminary study, but there are several improvements to be made for this interface to work successfully.

3.8.2 Impact of curvature on mucus production

To assess the differentiation and distribution of mucus producing cells on flat and curved membranes, ALI samples were stained with anti-mucin 5B, as shown on **figure 3.28**.

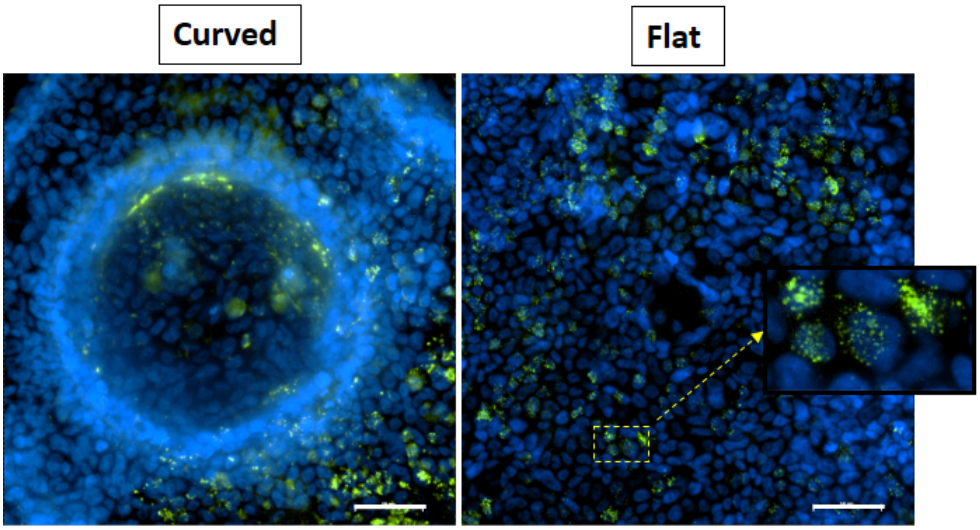

Figure 3.28: Mucus productive cells' distribution on curved and flat samples exposed to air (ALI). Immunostaining: DAPI for nuclei, MUC5B as goblet cells marker. Scale bar: 50 μm.

It is visible that goblet cells seem to be equally distributed on the flat membranes and inside the cavities which might indicate a non-specific expression of the protein in response to both ALI culture and curvature. In SEM images of the ALI samples (**figure 3.29**), it is possible to see an uniform and thin layer surrounding visible cells which might be produced mucus surrounding other cell layers and ECM formed after one month in culture.

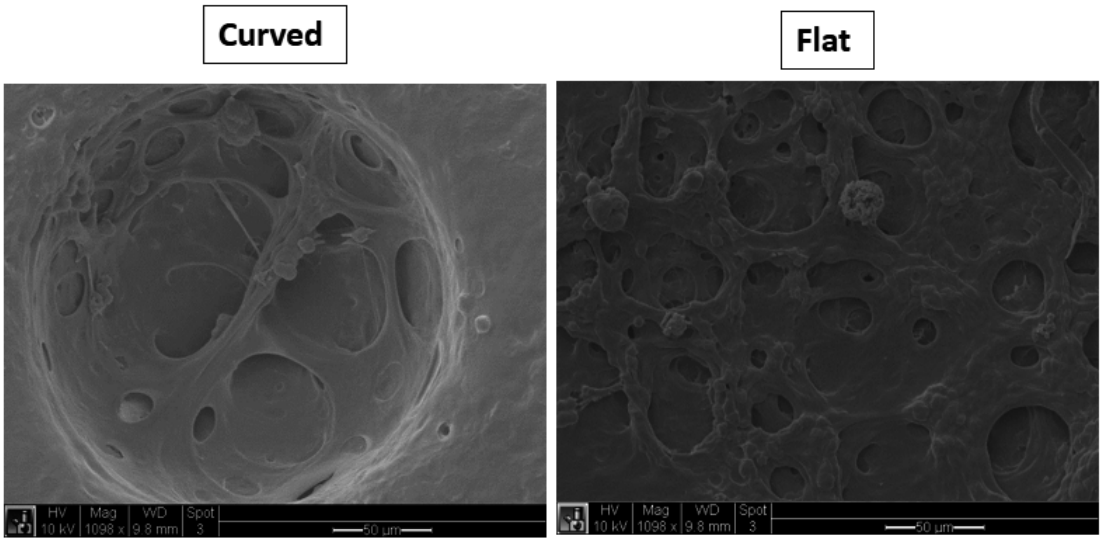

Figure 3.29: SEM images from curved (left) and flat (right) samples of ALI. Working distance: 10 mm, Beam voltage: 10 kV, Scale bar: 50 μm.

Mucus production by lung epithelial cells and their distribution on the cell barrier might be an indicator of their state, which might be useful for future implementation in lung disease models, such as the overproduction of mucin in chronic inflammatory lung disease [65].

4

Conclusions and Future Perspectives

4.1 Conclusions

As it is well known, polycarbonate is a suitable polymer for biomedical applications, more specifically for cell culture platforms. Do to its material properties, such as glass transition temperature of 148^{o}C [54] this material can be shaped into half-spherical cavities *via* gas-assisted microthermoforming. Different depths can be achieved by changing forming parameters like temperature and pressure. In order to produce approximately spherical cavities with a depth of 124,71 ± 5,05 μm, the temperature and pressure applied were 153^{o}C and 11 bar, respectively.

Furthermore, it is possible to modify these dense films into porous membranes, thermoformed or non thermoformed, *via* ion track etching. Its porosity (pores density and pore size) can be tuned and controlled by adjusting how long the process lasts. For thermoformed membranes, the pore size on the cavities starts as 3,01 ± 0,63 μm for 1 hour of etching and grows up to 11,39 ± 1,66 μm after 5 hours etching. On non-thermoformed membranes, after 1 hour of etching a diameter of 5,06 ± 0,32 μm is obtained, enlarging up to 8,81 ± 0,77 μm after 3 hours etching. These allow the creation of a substrate as similar as possible from the human alveoli, mimicking its dimensions and that will allow the communication between both sides of the membrane - epithelium and endothelium - once the co-culture is established.

A confluent monolayer was successfully formed when culturing lung epithelial cells on the PC membranes, allowing their adaptation, spreading and attachment inside cavity shaped substrates, which is the first positive result for the project. It was shown that the number of cells per area in the cavities is higher than on the flat substrates which might result in an advantage for a future cell barrier on the curved

surface. Also, it was shown that, in general, cells on curved surfaces tend to make more intercellular connections rather than on the flat membranes. CALU-3 are particularly know for creating strong tight junctions and if in contact with more cells per area by interacting in different angles, the cell layer is expected to be more cohesive which might have a positive impact on cell barrier formation, integrity and function.

Regarding cell proliferation, it was observed that cells cultured on cavities showed lower rates when compared to the flat membranes. However, it shouldn't be excluded from the study the regions in between cavities and around the array, that is, in fact, flat and might have an influence on the overall cell behaviour. It seems plausible to say that curvature influences cells' mitotic activity. This possible link between curvature and proliferation should be further investigated in regard of tissue regeneration.

Concerning cell apoptosis, results point out that cells on both curved and flat membranes presented low rates, which means that the membranes are not inducing cell death. Additionally, apoptosis was registered higher on curved membranes, which might indicate a possible link between curvature and apoptosis. Inside cavities, cells are forced to adapt different angles induced by curvature, becoming more rounded. This sensing of cell's extension or compression might culminate in apoptosis. This should be further explored and confirmed if it could be translated in cell renewal.

Even though CALU-3 metabolic activity was shown to be higher on curved membranes, the standard deviation associated to their metabolic activity on flat membranes and the ANOVA value calculated don't confirm the apparent difference to be significant. Comparing these results with the proliferation and apoptosis rates, this might represent a tendency to cells making extra effort to attach, spread and interact with neighbour cells but their survival is not inhibited. As expected, in general, cells cultured in the control have lower metabolic activity rates.

CALU-3 did not show problems when adhering to membranes' with cavities. In fact, they formed a strong monolayer with cell defined tight junctions, that could be observed through occludin staining. As remark, the incubation step (3 hours) after seeding is crucial for these cells to adhere to the surface.

For the air-liquid interface, the setup has to be optimised in order to obtain better results. In regard to cell barrier integrity, it was possible to see that a confluent and cohesive cell layer characterised by a great amount of tight junctions was formed, covering the total surface of the porous cavities. Regarding cell differentiation when

exposed to air, goblet cells distribution both on curved a flat membranes was observed. For the cilia, imaging techniques have to be improved.

In conclusion, a more realistic model of the human alveoli can be achieved by introducing porous cavities with desired dimensions and replacing the conventional 2 D flat membranes, which have little similarities with the structure to be modelled. Curvature influences epithelial cells by forcing them to assume a more natural behaviour seen *in vivo.* When confined to a curved microengineered structure, cells become rounded, surrounded by more neighbour cells, tight junctions are stronger and ECM adapts different spatial orientations, which is sensed by cells. This influences proliferation and apoptotic rates, cell-cell and cell-substrate interactions and cells' metabolic activity. Hopefully, these outcomes mimic real human alveolar phenomenons such regeneration, mucus secretion, cilia development and cell renewal.

4.2 Future Perspectives

To continue with this work and explore further results, future improvements should be performed mainly on the optimisation of the air-liquid interface. As soon as this is achieved, cells' expected differentiation when exposed to air can be maximised and successful assessments of the cell barrier's integrity with dextrans and transepithelial electrical resistance (TEER) measurements can be performed.

Once the ideal setup of porous curved membranes is produced, introducing it on a perfused system is the next step. In this first approach, the developed model is static but implementing it in a microfluidic chip allows an approximation to the human body's function, which should be taken as priority.

With this, it will be possible to obtain a more realistic "alveoli-on-chip", where the microenvironment can be controlled with defined culture medium and air flows, by introducing allergens and tobacco smoke and by attaching electrodes to continuously measure different parameters such cell barrier integrity, stretch and cilia movement.

Focusing on the cell composition itself, adding endothelial lung cells on the convex side of the cavity and macrophages (co-culture) allows a closer histological model, where it may be attempted oxygen-carbon dioxide exchange, as it happens in the air-blood barrier in the alveoli. Finally, replacing lung cancer cells lines by primary lung cells adds clinical relevance for future perspectives.

Bibliography

[1] P. Bove and S. Randell, *Comparative Anatomy of Normal Lung, Chapter 11: Comparative Mammalian Lung Primary Surface Epithelial Cell Culture*. 2009.

[2] E. R. Weibel, "Morphological Basis of Alveolar-Capillary Gas Exchange," no. 2, vol. 53, 1973.

[3] C. Gonçalves and V. Bairos, *Histologia, texto e imagens: Histologia Histogénese Organogénese - 2ª edição*. No. 978-989-8074-23-2, 2007.

[4] Fatehullah, Aliya, S. H. Tan, and N. Barker, "Organoids as an in vitro model of human development and disease," 2016.

[5] R. Truckenmüller, S. Giselbrecht, N. Rivron, E. Gottwald, V. Saile, A. van den Berg, M. Wessling, and C. van Blitterswijk, "Thermoforming of Film-Based Biomedical Microdevices," 2011.

[6] S. Giselbrecht, T. Gietzelt, E. Gottwald, C. Trautmann, R. Truckenmüller, K. F. Weibezahn, and A. Welle, "3D tissue culture substrates produced by microthermoforming of pre-processed polymer films," no. 10.1007/s10544-006-8174-8, 2006.

[7] K. L. Sellgren, E. J. Butala, B. P. Gilmour, S. H. Randell, and S. Grego, "A biomimetic multicellular model of the airways using primary human cells," no. 10.1039/c4lc00552j, 2014.

[8] T. C. Mertens, H. Karmouty-Quintana, C. Taube, and P. S. Hiemstra, "Use of airway epithelial cell culture to unravel the pathogenesis and study treatment in obstructive airway diseases," no. 10.1038/nmeth.3697, 2017.

[9] K. H. Benam, R. Villenave, C. Lucchesi, A. Varone, C. Hubeau, H.-H. Lee, S. E. Alves, M. Salmon, T. C. Ferrante, J. C. Weaver, A. Bahinski, G. A. Hamilton, and D. E. Ingber, "Small airway-on-a-chip enables analysis of human lung inflammation and drug responses *in vitro*," no. 10.1038/nmeth.3697, 2015.

[10] A. Jain, R. Barrile, A. D. van der Meer, A. Mammoto, T. Mammoto, K. D. Ceunynck, O. Aisiku, M. A. Otieno, C. S. Louden, G. A. Hamilton, R. Flaumenhaft, and D. E. Ingber, "Accepted Article: A primary human lung alveolus-on-a-chip model of intravascular thrombosis for assessment of therapeutics," no. 10.1002/cpt.742.

[11] D. Huh, B. D. Matthews, A. Mammoto, M. Montoya-Zavala, H. Y. Hsin, and D. E. Ingber, "Reconstituting Organ-Level Lung Functions on a Chip," no. 10.1126/science.1189401, 2010.

[12] A. M. Kloxina, K. J. R. Lewisa, C. A. DeForesta, G. Seedorf, M. W. Tibbitt, V. Balasubramaniam, and K. S. Ansetha, "Responsive culture platform to examine the influence of microenvironmental geometry on cell function in 3D," no. 10.1039/c2ib20212c, 2012.

[13] R. Edmondson, J. J. Broglie, A. F. Adcock, and L. Yang, "Three-Dimensional Cell Culture Systems and Their Applications in Drug Discovery and Cell-Based Biosensors," no. 10.1089/adt.2014.573, 2014.

[14] B. L. Pruitt, A. R. Dunn, W. I. Weis, and W. J. Nelson, "Mechano-Transduction: From Molecules to Tissues," no. 10.1371/journal.pbio.1001996, 2014.

[15] O. Y. F. Henry, R. Villenave, M. J. Cronce, W. D. Leineweber, M. A. Benz, and D. E. Ingber, "Organs-on-chips with integrated electrodes for trans-epithelial electrical resistance (TEER) measurements of human epithelial barrier function," no. 10.1039/c7lc00155j, 2017.

[16] J. E. Nichols, J. A. Niles, S. P. Vega, and J. Cortiella, "Novel in vitro respiratory models to study lung development, physiology, pathology and toxicology," no. 10.1186/scrt368, 2013.

[17] S. H, T. S, M. S, F. C, and Y. N, "Reconstruction of alveolus-like structure from alveolar type II epithelial cells in threedimensional collagen gel matrix culture," no. 142:783-792, 1993.

[18] H. MI, U. RE, K. K, P. K, and K. CJ, "Lung epithelial cell lines in coculture with human pulmonary microvascular endothelial cells: development of an alveolo-capillary barrier in vitro," no. 84:736-752, 2004.

[19] L. V. C, D. B, F. P, and L. KW, "Coculture of mesenchymal stem cells and respiratory epithelial cells to engineer a human composite respiratory mucosa," no. 10:1426-1435, 2004.

[20] Y. S. Zhang and A. Khademhosseini, "Seeking the right context for evaluating nanomedicine: from tissue models in petri dishes to microfluidic organs-on-a-chip," no. 10.2217/NNM.15.18, 2015.

[21] M. W. van der Helm, A. D. van der Meer, J. C. T. Eijkel, A. van den Berg, and L. I. Segerinkr, "Microfluidic organ-on-chip technology for blood-brain barrier research," no. 10.1080/21688370.2016.1142493, 2016.

[22] C. Luni, E. Serena, and N. Elvassore, "Human-on-chip for therapy development and fundamental science," no. 10.1016/j.copbio.2013.08.015, 2013.

[23] M. Wufuer, G. Lee, W. Hur, B. Jeon, B. J. Kim, T. H. Choi, and S. Lee, "Skin-on-a-chip model simulating inflammation, edema and drug-based treatment," no. 10.1038/srep37471, 2016.

[24] H. J. Kim, D. Huh, G. Hamilton, and D. E. Ingber, "Human gut-on-a-chip inhabited by microbial flora that experiences intestinal peristalsis-like motions and flow," no. 10.1039/C2LC40074J, 2012.

[25] Y. suke Torisawa, C. S. Spina, T. Mammoto, A. Mammoto, J. C. Weaver, T. Tat, J. J. Collins, and D. E. Ingber, "Bone marrow–on–a–chip replicates hematopoietic niche physiology in vitro," no. 10.1038/nmeth.2938, 2013.

[26] S. Sieber, L. Wirth, N. Cavak, M. Koenigsmark, U. Marx, R. Lauster, and M. Rosowski, "Bone marrow-on-a-chip: Long-term culture of human hematopoietic stem cells in a 3D microfluidic environment," no. 10.1002/term.2507, 2017.

[27] Y. Kang, T. Sodunke, J. Cirillo, M. Bouchard, and H. Noh, "Liver on a chip: Engineering the liver sinusoid," no. 10.1109/Transducers.2013.6626762, 2013.

[28] B. R., G. L., M. M., L. C., and L. E., "Development of a renal microchip for in vitro distal tubule models," no. 10.1021/bp0603513, 2007.

[29] D. Huh, D. C. Leslie, B. D. Matthews, J. P. Fraser, S. Jurek, G. A. Hamilton, K. S. Thorneloe, M. A. McAlexander, and D. E. Ingber, "A Human Disease Model of Drug Toxicity–Induced Pulmonary Edema in a Lung-on-a-Chip Microdevice," no. 10.1126/scitranslmed.3004249, 2012.

[30] B. M. Maoz, A. Herland, O. Y. F. Henry, W. D. Leineweber, M. Yadid, J. Doyle, R. Mannix, V. J. Kujala, E. A. FitzGerald, K. K. Parker, and D. E. Ingber, "Organs-on-Chips with combined multi-electrode array and transepithelial electrical resistance measurement capabilities," no. 10.1039/C7LC00412E, 2017.

[31] R. Truckenmüller, S. Giselbrecht, and et al., "Flexible Fluidic Microchips Based on Thermoformed and Locally Modified Thin Polymer Films.," no. 125, 2008.

[32] K. Pinkerton, L. V. Winkle, and C. Plopper, *Comparative Anatomy of Normal Lung, Chapter 1: Overview of Diversity in the Respiratory System of Mammals.* 2015.

[33] J. Polak, S. Mantalaris, and S. E. Harding, *Advances in Tissue engineering.* 2008.

[34] A. M. Pinto and C. R. Cordeiro, *Fisiopatologia - Fundamentos e Aplicações.* 2009.

[35] S. Reynolds, K. Pinkerton, and A. Mariassy, *Comparative Anatomy of Normal Lung, Chapter 6: Epithelial Cells of the Trachea and Bronchi.* 2009.

[36] S. Matthes, R. Hadley, J. Roman, and E. White, *Comparative Anatomy of Normal Lung, Chapter 20: Comparative Biology os the Normal Lung Extracellular Matrix.* 2009.

[37] S. E. Dunsmore and D. E. Rannels, "Invited Review: Extracellular matrix biology in the lung," no. 1040-0605/96, 1996.

[38] Y. Zhu, A. Chidekel, , and T. H. Shaffer, "Cultured Human Airway Epithelial Cells (Calu-3): A Model of Human Respiratory Function, Structure, and Inflammatory Responses," 2010.

[39] J. Lee, M. J. Cuddihy, and N. A. Kotov, "Three-Dimensional Cell Culture Matrices: State of the Art," 2008.

[40] M. Ravi, V. Paramesh, S. Kaviya, E. Anuradha, and F. P. Solomon, "3D Cell Culture Systems: Advantages and Applications," 2008.

[41] V. Weaver, O. Petersen, F. Wang, C. Larabell, P. Briand, C. Damsky, and M. Bissell, "Reversion of the Malignant Phenotype of Human Breast Cells in Three-Dimensional Culture and In Vivo by Integrin Blocking Antibodies," 1997.

[42] K. Bhadriraju and C. Chen, "Engineering cellular microenvironments to improve cell-based drug testing," no. 10.1016/S1359-6446(02)02273-0, 2002.

[43] A. Birgersdotter, R. Sandberg, and I. Ernberg, "Gene expression perturbation in vitro—A growing case for three-dimension (3D) culture systems," no. 10.1016/j.semcancer.2005.06.009, 2005.

[44] R. Truckenmüller, S. Giselbrecht, and et al., "Materials, Microfabrication and Design - Fabrication of Advanced Microwell Arrays for Perfused 3D Cell Culture in Microfluidic Bioreactors," no. 509, 2010.

[45] D. Huh, G. A. Hamilton, and D. E. Ingber, "From 3D cell culture to organs-on-chips," no. 10.1016/j.tcb.2011.09.005, 2011.

[46] E. Knight and S. Przyborski, "Advances in 3D Cell Culture Technologies Enabling Tissue-like Structures to be Created in vitro.,"

[47] H. T.-L. Nguyen, S. T. Nguyen, and P. V. Pham, "Concise Review: 3D Cell Culture Systems for Anticancer Drug Screening," 2016.

[48] S. G. e. a. Christine Richter, Martina Reinhardt, "Spatially Controlled cell Adhesion on Three-dimensional Substrates.," no. 125, 2008.

[49] L. G. Johnson, "Applications of imaging techniques to studies of epithelial tight junctions," 2004.

[50] J. Wanga, P. Yi, Y. Denga, L. Penga, X. Lai, and J. Ni, "Recovery behavior of thermoplastic polymers in micro hot embossing process," no. 10.1016/j.jmatprotec.2016.12.024, 2016.

[51] C. Richter, M. Reinhardt, S. Giselbrecht, D. Leisen, V. Trouillet, R. Truckenmüller, A. Blau, C. Ziegler, and A. Welle, "Spatially Controlled Cell Adhesion on Three-dimensional Substrates,"

[52] P. A.Gunatillake and R. Adhikari, "Biodegradable Synthetic Polymers for Tissue Engineering," 2003.

[53] G. Tjandraatmadja and L. Burn, "The effects of ultraviolet radiation on polycarbonate glazing," 1999.

[54] J. Ong, Y. Koh, and Y. Fu, "Microlens array produced using hot embossing process," 2001.

[55] C. M. Agrawal and R. B. Ray, "Biodegradable polymeric scaffolds for musculoskeletal tissue engineering," 2000.

[56] D. G. Powell, "Medical Applications of Polycarbonate . Medical Plastics and Biomaterials Magazine," 1998.

[57] Z. Siwy, P. Apel, D. Dobrev, R. Neumann, R. Spohr, C. Trautmann, and K. Voss, "Ion transport through asymmetric nanopores prepared by ion track etching," no. 10.1016/S0168-583X(03)00884-X, 2003.

[58] P. Apel, "Invited talk: Track etching technique in membrane technology," 2001.

[59] P. Y. Apel, I. Blonskaya, S. Dmitriev, O. Orelovitch, and B. Sartowska, "Structure of polycarbonate track-etch membranes: Origin of the "paradoxical" pore shape," no. 10.1016/j.memsci.2006.05.045, 2006.

[60] C. Grainger, L. Greenwell, D. Lockley, G. Martin, and B. Forbes, "Culture of Calu-3 Cells at the Air Interface Provides a Representative Model of the Airway Epithelial Barrier," 2006.

[61] M. E. Kreft, U. D. Jerman, E. Lasic, N. Hevir-Kene, T. L. Rizner, L. Peternel, and K. Kristan, "The characterization of the human cell line Calu-3 under different culture conditions and its use as an optimized in vitro model to investigate bronchial epithelial function," 2014.

[62] R. I. Freshney, *Culture of Animal Cells: A Manual of Basic Technique and Specialized Applications*. 2010.

[63] N. Wang, J. P. Butler, and D. E. Ingber, "Mechanotransduction across the cell surface and through the cytoskeleton.," no. 10.1126/science.7684161, 1993.

[64] C. S. Chen, M. Mrksich, S. Huang, G. M. Whitesides, and D. E. Ingber, "Geometric Control of Cell Life and Death," no. 10.1126/science.276.5317.1425, 1997.

[65] H.-P. Hauber, S. C. Foley, and Q. Hamid, "Mucin overproduction in chronic inflammatory lung disease," 2006.

Index

Appendices

A

Human Pulmonary Alveolar Epithelial Cells Study

A.1 HPAEC Growth Curve

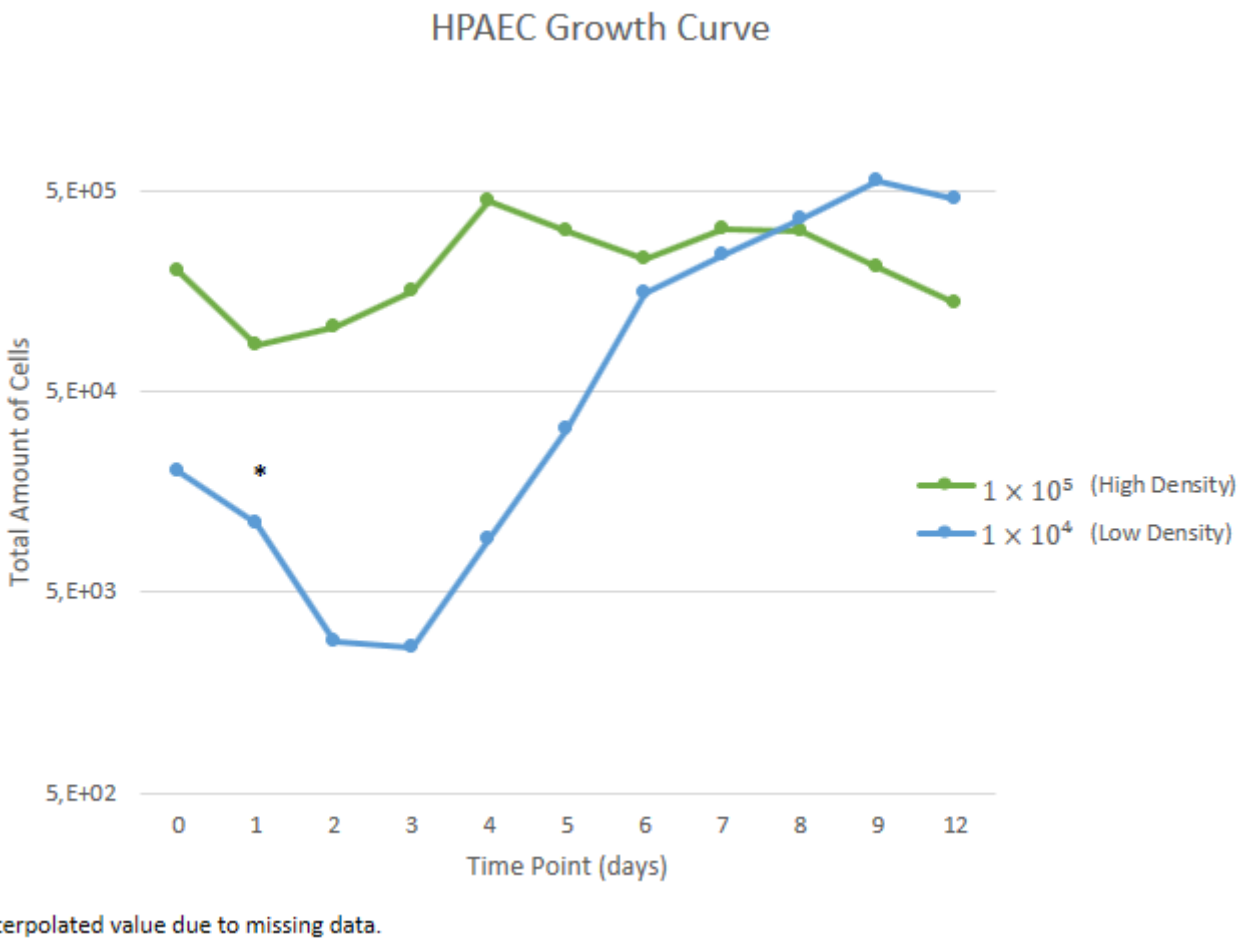

Figure A.1: Growth curve for two different cell densities of the Human Pulmonary Alveolar Epithelial Cells. Missing data represented as an interpolation.

As a first approach to the graphic's analysis, it is possible to see the characteristic growth pattern defined by the lag phase, the exponential phase and the stationary or *plateau* phase for both cell densities. In the first and third days after cell seeding, high and low density, respectively, show a decrease in the total cell number, which is a characteristic behaviour of the lag phase. Then, an exponential growth happens followed by a maintenance of constant cell number, the *plateau* phase. Starting with the considered "low density" of a cell concentration of 1×10^4 cells/well , the number of cells highly decreases in the first three days, followed by an exponential increase from day three to day nine, slowing down its growth rate from day six and achieving the possible *plateau* stage by day twelve. For the cell concentration of 1×10^5 cells/well considered as "high density", the amount of cells in culture reduces 24 hours after cell seeding, an exponential growth is represented from day one to day four, maintaining the cell number mostly constant from that day to day eight and decreasing its number after that due to possible cell death. By direct observation of the graphic, HPAEC seeded with the considered "high density" start proliferating and increasing their cell population two days before the cells sub cultured with a "low density". One parameter that can be taken from this phase by plotting the adjusted equation, is the the *population doubling time*. For the "high density", the doubling time, *i.e*, the required time for the cell population to double their number, is 31,08 hours while, for the "low density", it takes 18,37 hours, less than one day.

To take into account that the cell number for the first day of the "low density" counting is an interpolated value because data was missing. The fact that the cell number for this density was reduced from the beginning, and since the amount of cells typically decreases in the first days, it was tricky to count the total number of cells in culture one day after seeding, ending up losing the sample for this time point.

Plotting the growth curve of different cells is one of the methods to measure cell proliferation based on the semi-log plot of the cell number in subculture over time. Knowing the cell proliferation rates is extremely useful to determine the response of cells to different stimulus [62]. Since the lag phase is the period for cell adaptation after cell seeding, it shows a decrease in the total amount of cells for both densities. In this phase, cells replace elements of their surface and ECM lost during trypsinization, proceed to attach to the substrate and spread out [62]. For the high density, the lag phase happens for the first 24 hours, which is a very short period. This might mean that for this cell density, the attachment and survival rate is bigger. On the other hand, for the low density the lag phase lasts longer, which may imply cell adaptation or cell loss. Progressing to the period of exponential cell growth,

it is more accentuated and it lasts longer for the "low density" than for the "high density" This period finishes one or two population's doubling after cells achieving confluence [62], *i.e*, once all the available surface area for cell growth is occupied. At this moment, all cells are in contact with surrounding cells, the growth rate falls to 0-10% and cell proliferation ceases almost completely [62]. Since the HPAEC are epithelial cells, they stop growing after reaching confluence, remaining as a monolayer [62]. Furthermore, on day 12, the automatic cell counter showed a decrease in the cell viability from the usual 98-100% to about 70%.

Two parameters can be taken from this phase: the saturation density (number of cells per cm^2 of growth surface) and the *plateau* level (number of cells per millimetre of medium) which, by the graphic observation seems apparently similar but it is extremely difficult to measure them accurately [62]. However, it is noticeable that a cell concentration of $1x10^5$ to cell seeding is already too high, resulting in a saturation and almost reaching confluence by day one. Regarding the general aspect of the HPAEC growth curve and based on literature [62] it seems like the "low cell density" represents a reduced survival behaviour, for the cell number decrease in the first 3 days but followed by a huge population growth in the following days. By contrast, the "high cell density" shows a profile of lower saturation density. Depending on the pretended use of the cells, the adequate cell density has to be chosen. If the cells are needed in the shortest time possible it is a good option to seed cells at a higher density. On the other hand, if a proliferation study is being performed, a lower density is a better choice so that cells have enough time to grow and spread. For these reasons, a cell density around $1x10^4$ was the chosen one to the preliminary experiments using HPAEC.

A.2 Impact of curvature on lung primary cells' metabolic activity

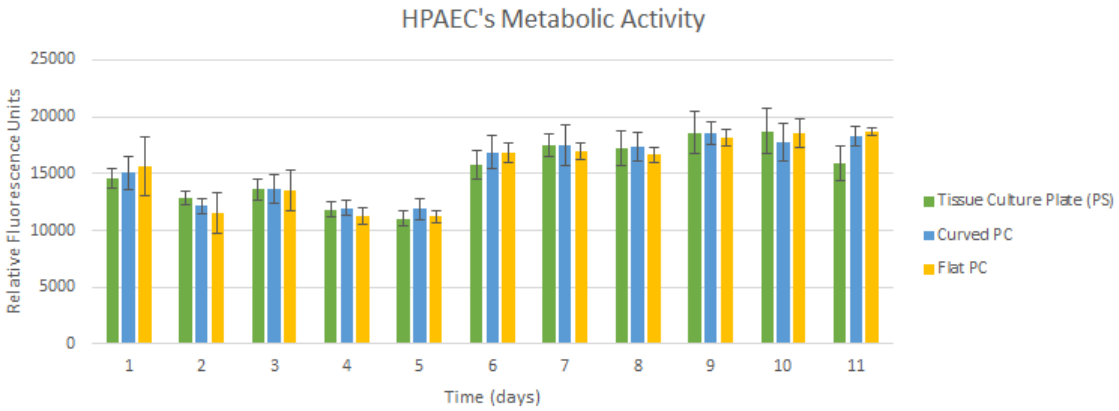

Figure A.2: HPAEC's metabolic activity measured for 11 days in three different substrates: polysterene and PC curved and flat. Tissue culture well's area normalised. ($p>0.05$).

Comparing this result with the CALU-3 it is visible that metabolic activity is much higher in the primary cell culture. However, the differences between conditions is not as accentuated as in the CALU-3. Metabolic activity is slightly higher in the curved membranes instigating that cells might need extra cell activities to adapt to the new conformation and confirming the pattern studied in the CALU-3. Until day 5 it's visible a decrease in the overall metabolic activity, possibly by dying while adapting to the coated substrate, but the fact that it is common to all three substrates is a positive result. After day 6, HPAEC maintain their metabolic activity constant for all conditions.

However, statistical analysis with ANOVA confirms that the differences for curved and flat are not statistically significant which might suggest that these values simply follow a tendency.

A.3 Air liquid interface: membrane's permeability

Permeability to two completely different molecular weighted dextrans (a small dimensioned of 3 kDa and a big one of 70 kDa) was measured on an ALI with HPAEC

(primary alveolar pulmonary cells). The same limitations in the set up were faced, so the results were similar to the observed in the ALI with CALU-3.

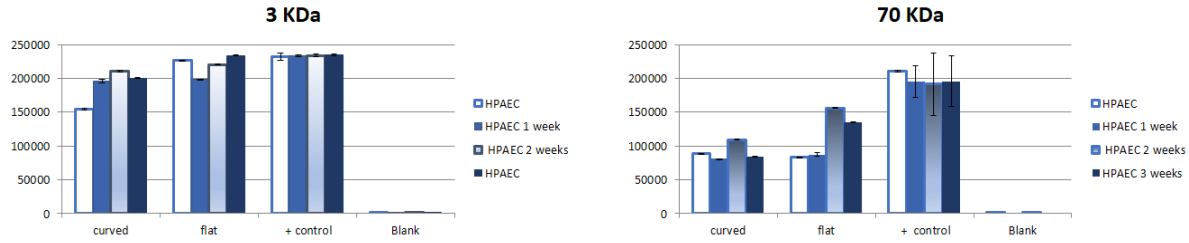

Figure A.3: Cell barrier permeability and integrity assessment for HPAEC cultured in an air-liquid interface. Measurements were taken weekly for 4 weeks. Area normalised.

Starting with the lower molecular weight, it is possible to see on the left graphic of **figure A.3** that permeability to molecules of 3 kDa is similar to both CALU-3 and HPAEC.

For the higher molecular size shown on the right graphic of **figure A.3** it is possible to see that, in general, less dextran passes through the primary cell barrier, when compared to the CALU-3 results. From these results, it is possible to make an assumption that primary cells are able to form a tight cell barrier when exposed to air, like the CALU-3, with possibly smaller gaps in between cells, making a more cohesive barrier.

B

CALU-3 complementary study

B.1 Impact of curvature on regeneration

The rationale of the trial was how do cells behave after a physical aggression in curved and flat surfaces correlating it with an alveolar injury *in vivo*. The two discussed and chosen approaches were scratching the cell layer with a needle and putting a drop of trypsin so that some would detach, and see how long would it take to close the created gap in the cell colony.

It was firstly attempted to scratch with the smallest materials we had in the laboratory. Under the inverted microscope it was tried to enter the cavities with a 10μL micro pipette tip, a 0,7x30mm needle and a 0,3x12mm needle. The first referenced was discarded right away because its diameter was to big to get to the bottom of the cavity. Both needles were able to enter the cavities and reach the bottom but since the depth of the cavities is around 150μm it is very difficult to control the hand movement and to only scratch the cell layer without ripping the membrane apart.

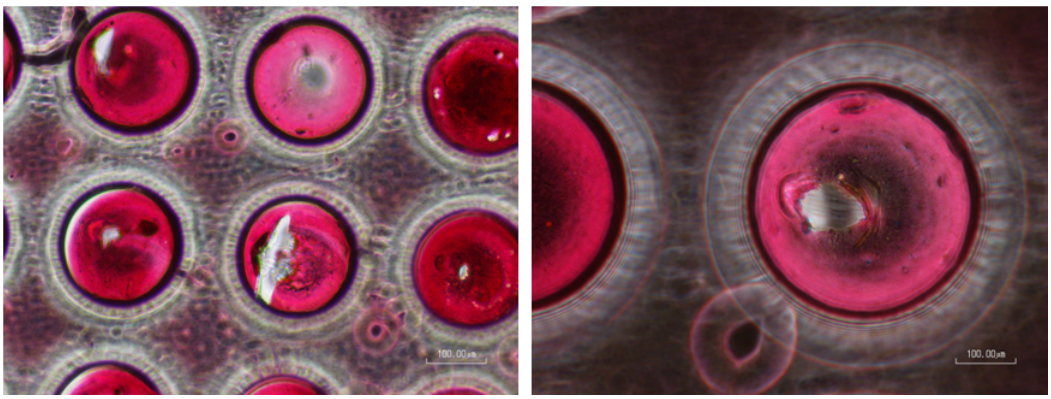

Figure B.1: The bottom of the cavities was coloured with a marker to make it easier to see the scratch. As it may be seen in the images, the membrane is torn apart instead of only scratching the possible existent cell layer.

For the trypsinization, it was tested the procedure with water and trypan blue first. The drop using a micro pipette tip got the entire array soaked instead of entering only one cavity. With the smallest needle, even though the immediately formed drop in the tip of it is small and adequate to enter the cavity, it grows bigger to compensate all the tension and surface forces and achieve equilibrium, soaking the neighbour cavities as it happen previously.

Both attempts did not succeeded and even though it would be very interesting to study and analyse the cell regeneration and growth after an injury, since more experiments were planned, optimising the scratch assay and buying all the needed material would take a long time.

B.2 ALI culture: β-tubulin immunostaining

Even though the immunostaining for mucin, phalloidin and occludin worked nicely in the ALI culture samples, the same didn't happen for β-tubulin, which filaments' and respective orientation couldn't be seen with the 40X magnification with oil objective lens from the live cell microscope. Image visualisation in the confocal would probably allow to see these structures.

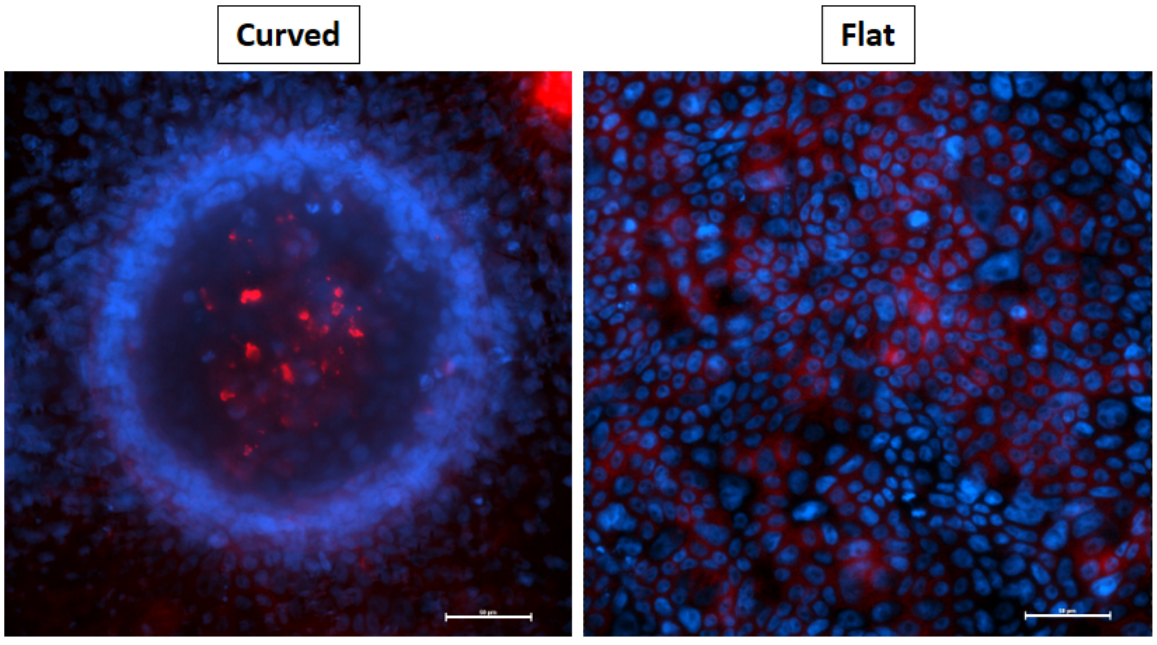

Figure B.2: Attempt to mark tubulin fillaments characteristic from lung cells' cilia. Low magnification to see any important detail or orientation. Immunostaining: DAPI, β-tubulin. Scale bar: 50μm.